Gas vertex detectors

N. M. Nikityuk
Joint Institute for Nuclear Research, Dubna

Fiz. Élem. Chastits At. Yadra **29**, 1499–1544 (November–December 1998)

The evolution and current status of the technique of three-coordinate vertex detectors are reviewed. Data acquisition methods and the recording of the topology of complicated events by means of vertex detectors are discussed, along with the features of such detectors as time-projection chambers, pictorial (jet) chambers, vector drift chambers, and vertex detectors based on straw tubes. Tables of the parameters of the best known gas vertex detectors used in fixed-target and colliding-beam experiments are given. © *1998 American Institute of Physics.* [S1063-7796(98)00506-3]

INTRODUCTION

After the discovery of the J/ψ particle in November, 1974, a new stage in the development of elementary-particle physics began: the use of electronic methods and the accelerator technique, required to study the properties of short-lived particles with lifetime less than 10^{-8} sec. In the accepted classification according to lifetime,[1] elementary particles and resonances are divided into three groups: (1) long-lived particles with lifetime longer than 10^{-8} sec. Created in high-energy collisions, they have a decay length of order 1 m and larger ($K^{\pm},\pi^{\pm},\mu^{\pm},\ldots$). The detection and observation of such particles using ordinary track detectors presents no particular difficulty, and they can be identified using Čerenkov counters; (2) neutral particles ($\gamma,K_L^0,n,\ldots$) observed using calorimeters; (3) particles with lifetime of order 10^{-10} sec ($K_s^0,\Sigma^{\pm},\Lambda,\ldots$), whose study does not require the use of vertex detectors. Beginning in the mid-1970s, a wide range of problems in elementary-particle physics arose in connection with the study of the properties of short-lived particles with lifetime $<10^{-11}$ sec.

For example, the family of elementary particles including the τ lepton, hadrons, and charmed and bottom particles with lifetime 10^{-12}–10^{-13} sec is of particular interest. The decay lengths of these particles are hundreds of microns. They are detected and identified using installations containing vertex detectors. The primary decay vertex is usually accompanied by two or more secondary vertices located a distance L from each other. The typical value of L is hundreds of microns[1] (see Fig. 1). It would appear that the lifetime τ could be found accurately by directly measuring L and the characteristics of the decay products. However, this method is hardly used at present for several reasons: the high level of background in the experiments and the extracted high-energy beams used at colliders; the impossibility of directly measuring the coordinates of the primary decay vertex, which lies inside the beam pipe where the colliding beams intersect; and the impossibility of determining the particle momentum in the case of neutral-particle decay. Therefore, the coordinates of the decay vertex are determined by an indirect method based on measuring the impact parameter of each track (Fig. 2). The impact parameter is the distance h by which a track from the secondary decay vertex, when extrapolated backward, deviates from the primary vertex. It is important that the value of this parameter is independent of the particle momentum, and so it can be used both to determine the coordinates of the decay vertex, and to measure the lifetimes of short-lived particles.[2] The possibility of using the impact parameter to find the coordinates of particle decay vertices was first demonstrated in Ref. 3. Owing to the small lifetime τ, the accuracy of measuring the impact parameter, especially near the target, must be tens of microns or even a few microns. Various types of detectors are used to achieve this accuracy: photoemulsion plates, bubble chambers, high-precision gas detectors, semiconductor vertex detectors, and also vertex detectors based on scintillating fiber-optics light guides (SCIFIs).

The high accuracy attainable in bubble chambers allows the direct observation and measurement of the parameters and topology of events involving short-lived particles. For a bubble diameter of 20 μm the two-track resolution is 20 μm, and the accuracy of measuring the coordinate of a point along the track is 5 μm. A similar accuracy is obtained using the photoemulsion technique, but there the rate at which statistics are accumulated is rather low and, moreover, it does not permit the use of electronic methods for selecting and reconstructing useful events by means of multilevel trigger

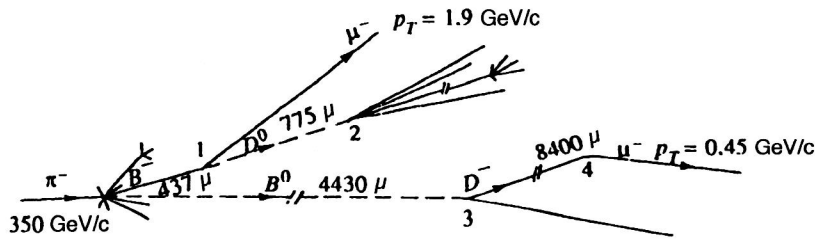

FIG. 1. Topology of a typical event containing several decay vertices (for π^0 mesons of energy 350 GeV/c); μ stands for micron. The event was recorded using emulsion.

systems which record and filter the physical information. Therefore, electronic and electronic–optical methods are used in current and planned experiments at high and superhigh energies. Multicell three-coordinate drift detectors, various modifications of semiconductor detectors, and SCIFI detectors are used as the vertex detectors.

In Table I we compare the parameters of various types of vertex detector.

The response of time-projection chambers (TPCs) is mainly determined by the drift time, and, owing to the large drift gap, the electron drift time is tens of microseconds. Therefore, the information recorded by a TPC cannot be used to organize a fast first-level trigger. Chambers of the jet type with time expansion using multidrift and straw tubes have an order-of-magnitude higher response rate compared to TPCs, and so they do not impose constraints on the recording electronics. The other types of detector have a high response rate, but it is difficult to realize in practice owing to the large number of data channels. Therefore, data readout from microstrip detectors is usually done using multiplexers. The data readout from CCD matrices and SCIFIs is sequential, and so it takes tens of milliseconds.

The goal of this review is to systematize, in a compact form, the numerous publications devoted to precision gas vertex detectors, the electronic readout systems associated with them, and the specialized processors for detecting decay vertices and calculating the impact parameter. In addition to this introduction, there are six sections and a conclusion. In the first section we discuss the techniques used in fixed-target and colliding-beam experiments. In the second we briefly consider the evolution and properties of three-dimensional gas detectors. In the third we describe the construction and characteristics of the best known time-projection chambers. The fourth section is devoted to jet chambers, which are faster and more accurate than TPCs. In the fifth section we describe vector vertex detectors and time-expansion chambers. The sixth section deals with the possibilities offered by gas vertex detectors in which multidrift and straw tubes are used.

FEATURES OF THE TECHNIQUES USED IN FIXED-TARGET AND COLLIDING-BEAM EXPERIMENTS

There are two types of high-energy physics experiment performed at accelerators. In the first, an accelerated beam of particles interacts with a stationary target (fixed-target experiments). Under these conditions the energy in the center of mass grows as the square root of the beam energy. Most

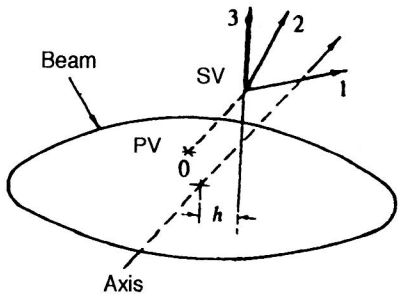

FIG. 2. Determination of the impact parameter h in the case where the coordinate of the primary decay vertex (PV) is unknown; 1, 2, 3 are the coordinate axes. SV is the secondary decay vertex.

of the interaction products leave the target at a small angle relative to the beam axis. The second type of experiment uses colliders, where accelerated particles circulate in opposite directions and collide inside the small beam-intersection region. The energy in the c.m. frame grows linearly with the beam energy. Experiments of this type will be important in future research. The beam energy attained at present at the proton–proton collider in the United States (Fermilab) is 1 TeV.

Fixed-target experiments at energies in the TeV range have the following features: all tracks concentrated in a small angle of order 100 mrad; high multiplicity of recorded tracks in an event; a high rate of recording events (several hundred kHz); and large particle momentum. Owing to the latter features, in some cases it is possible to neglect multiple scattering, and then a vertex detector can consist of several hodoscopic planes with high spatial resolution arranged perpendicularly to the beam with known distance from the first plane to the target. This distance must be of order $\gamma c\tau$, where γ is the relativistic factor, c is the speed of light, and $\tau \sim 10^{-13}$ sec is the characteristic lifetime of a charmed particle.

From the viewpoint of experimental technique, collider experiments differ from fixed-target experiments in several respects. (1) Since the particles collide in the c.m. frame, they can be emitted isotropically, and so the detector must cover all or most of the interaction space. (2) The multiplicity of particles created in a collision grows significantly with energy and can reach 100 and more. The jet phenomenon is observed, where near the target there are sets of particle tracks diverging from each other by small angles. (3) Since the interaction point is located inside the beam pipe, its coordinate can be determined only by extrapolating the recorded tracks. The typical length of the interaction region

TABLE I. Comparison of the parameters of vertex detectors.

	DETECTOR					
Parameter	TPC*	Jet†	Multidrift tubes	Microstrip	CCD	SCIFI
Spatial resolution, μm	200	20–100	10–50	2–20	3–5	25
Two-track resolution, μm	2500	35–500	–	50–60	40–50	52
Accuracy of impact-parameter determination, μm	–	35–100	35–100	40	30	10

*TPC stands for time-projection chamber.
†Jet chambers are gas microvertex detectors (see below).

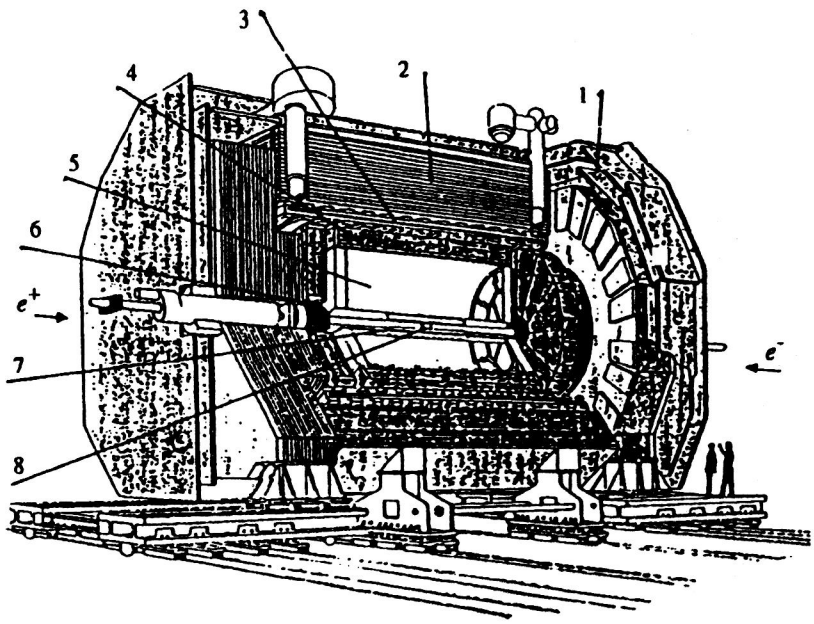

FIG. 3. Schematic depiction of the ALEPH setup: (1) muon chambers; (2) hadron calorimeter; (3) superconducting magnet; (4) electromagnetic calorimeter; (5) time-projection chamber; (6) beam indication system; (7) inner tracking chamber; (8) precision vertex detector.

along the beam direction (z coordinate) is 50 cm, and its cross section dimension is 1 mm. (4) The track curvature, which is smaller than in fixed-target experiments, does not allow particle multiple scattering to be neglected. (5) The problem arises of radiation stability of the electronics located near the beam pipe. These and other factors affect the complexity of the physical setup as a whole—its configuration, and the methods of processing the track information and identifying particles. Therefore, a vertex detector is essentially composed of individual detectors operating on different principles and having different resolutions and sizes. As an example, in Fig. 3 we schematically show the ALEPH installation, designed for experiments at CERN.[4] The installation contains several individual and rather complex detectors which perform specific functions. The beam pipe in which e^+ and e^- beans collide passes through the center of the setup. The typical diameter of the beam pipe is 2.5 cm. The tracking system includes three detectors: a vertex detector consisting of two layers of microscrip detectors with two-sided readout, a drift chamber of outer radius 35 cm, which also forms a part of the trigger system, and a time projection chamber of outer radius 125 cm. A gas chamber of the jet type was initially used instead of a semiconductor vertex detector. It should be noted that two types of detector are used here; they will be described in more detail in the following sections. The first is located directly at the beam pipe, where the track density is highest. This is the so-called jet chamber, which performs the functions of a precision microvertex detector. CCD matrices have also recently been used as microvertex detectors. A TPC (of outer diameter 2 m) is used to record tracks located far from the primary decay vertex. The TPC is located in a magnetic field, which is necessary for measuring track curvatures. The installation also contains several detectors used to obtain auxiliary information. For example, calorimeters are used to measure the particle energy, and hodoscopic calorimeters to measure the coordinates and sizes of clusters.

Precision detectors will also play an important role in future experiments at the Large Hadron Collider (LHC). As pointed out in Ref. 5, there are two reasons for detecting decay vertices: to separate the primary decay vertex in events with high multiplicity, and to separate the primary and secondary decay vertices containing short-lived particles.

Vertex detectors receive a great deal of attention in the

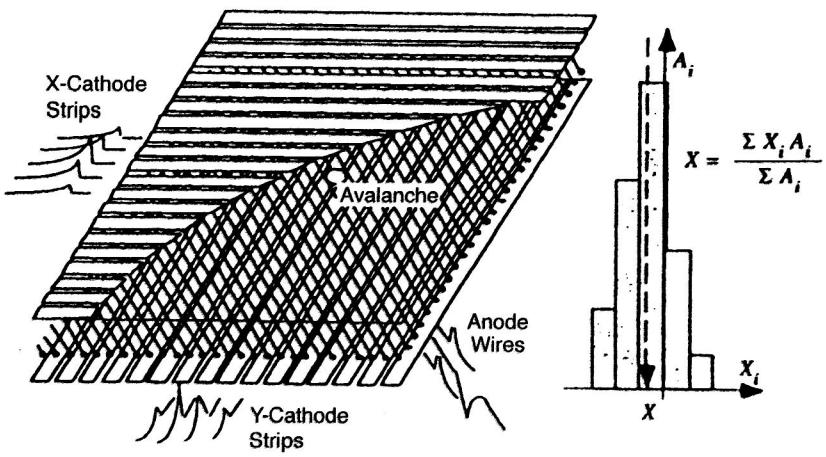

FIG. 4. MWPC with readout of positive-parity signals from the cathode plane. The method of determining the center of gravity of the avalanche is shown on the right.

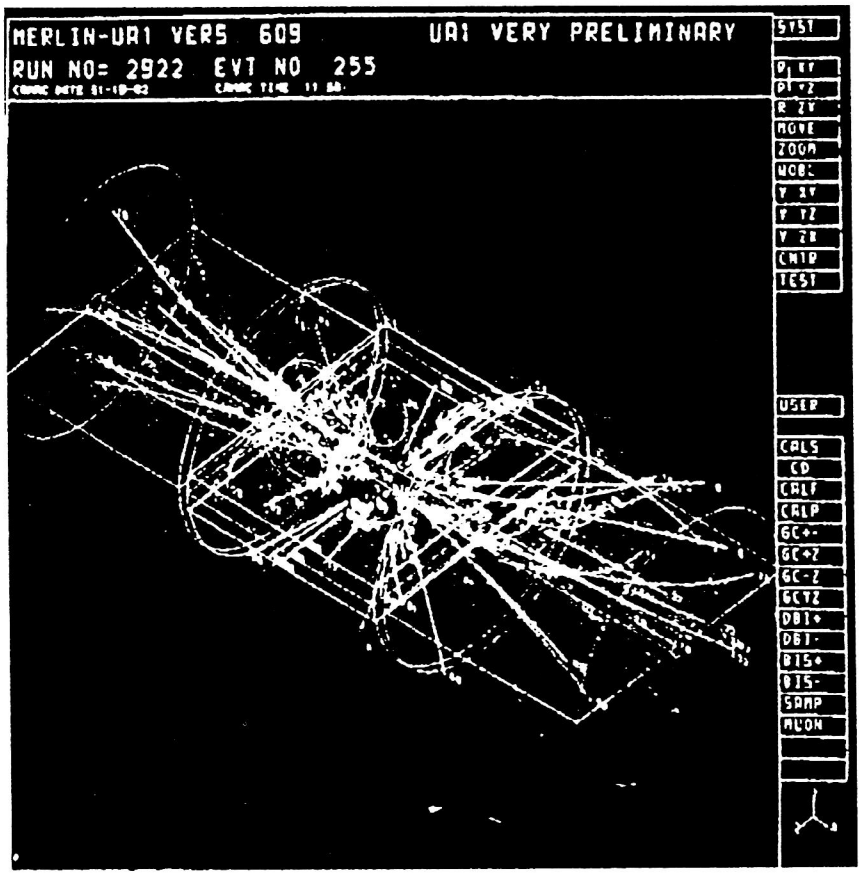

FIG. 5. A complicated event recorded using a time-projection chamber (display image after computer processing).

Western literature. The author of Ref. 2 discusses various aspects of the technique for measuring the lifetimes of short-lived particles and studying the physics of processes leading to event topologies containing primary and secondary decay vertices, and gives examples of the use of various types of vertex detector. The author of Ref. 1 gives a detailed treatment of the physics of semiconductor detectors and their use as vertex detectors, and discusses the problems of radiation stability and the fundamental limitations on the accuracy of measuring particle tracks. He also gives examples of the construction of various types of semiconductor vertex detector and methods of data acquisition. Finally, the various requirements imposed on vertex detectors designed for both fixed-target and collider experiments are studied in Ref. 6.

THREE-COORDINATE GAS DETECTORS

Of the coordinate detectors used in the 1970s, the most popular were multiwire proportional chambers (MWPCs). These became the classical type of detector. They are described in detail in Ref. 7. The idea of cathode readout proved especially fruitful. This method merits detailed discussion, because it is widely used in modern three-coordinate gas detectors. A signal of positive polarity is fed to the cathode plane of the MWPC; this cathode plane can consist of wires, strips, or groups of wires (Fig. 4). These electrodes are used to measure the induced charge, the center of which coincides with the center of the electron cloud arising as a result of the ionization of the gas filling the chamber by a charged particle. It is important that the amplitude and time evolution of the pulses induced at the strips depend on the position of the electron avalanche relative to the cathodes. This phenomenon is used to measure the spatial location and, accordingly, the second coordinate of the particle interaction with a high accuracy of up to 30 μm, because the analog signals are digitized using precision ACDs (more than 10 bits).[8] Further improvement of MWPCs made it necessary to identify complex events with high multiplicity and high track density. The drift chamber was thus born. By measuring the time for electrons to drift between signal wires, one of the track coordinates can be measured with high accuracy.[9] Therefore, in a three-dimensional gas detector, one coordinate of the particle trajectory is the position of the signal wire, and another is the location of the center of the avalanche induced at the cathode strips. The third is calculated from the drift time of the electron avalanche. One of the

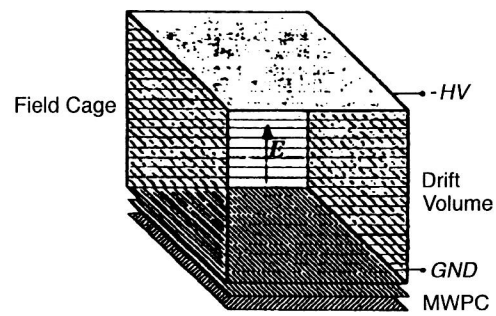

FIG. 6. Schematic depiction of a rectangular time-projection chamber.

TABLE II. TPC parameters.

Characteristic	Setup					
	HISS [20]	PEP-4 [10.11]	ALEPH [26–29]	TOPAZ [17–18]	DELPHI [23–25]	CDF [32]
Diameters, cm:						
outer	–	180	360	260	280	
(active)					116	21
inner	–	31	70	–	120	
(active)					32.5	7
Length, cm	–	200	220	300	2×150	
(active)					2×134	35.3
Size of cathode plane, m^2	1.5×1	–	–	–	–	
Number of readout elements (pads)	120×128	13824	44000	4096	2×10^4	
Pad size, mm^2	12×8	7.5×75	6.2×30	12×10		4.12×4
Spatial resolution, μm	–	100±3	150±5	–	–	
Pressure, atm	1	10	1	3	4	1
Drift distance, cm	2×75	2×1	2×20	2×20	368	15.25
Frequency of sampling dE/dx, MHz	100	10	11.4	1.4	14	10.6
Gas multiplication factor	3000	–	–	–		
Magnetic field, kG	13	13	1T	1T	12	1.5T
Working voltage, kV				–	−50	
Electric field, V/cm	120	–	260	–	150	320
Number of data channels	15360	16020	5×10^3	–	–	3072
Two-track resolution	2.5	–	–	–	1.5	
Drift velocity, μm/nsec	50	70	–	–	64	46
Drift time, μsec	75	–	–	24	20	3.5
Number of MWPC wires	–	2196	6336		2300	
Gas mixture	90% Ar +10%CH_4	80% Ar +20%CH_4	91% Ar +9%CH_4	90% Ar +10%CH_4	80% Ar +20%CH_4	50% Ar +50%CH_4

Note: minus (−) means that there is no data.

coordinates is often determined by dividing the charge induced on a resistive sense wire or by means of a delay line. An important feature of drift chambers is that they can have various shapes. Cylindrical drift chambers are the most widely used. The difficulty associated with the left–right ambiguity arising when drift chambers are used to identify particle tracks is resolved by introducing an additional plane or by other constructional methods (see below). Therefore, drift chambers, primarily, those with large drift gap, have served as prototypes of three-coordinate gas detectors, which at present include time-projection chambers, jet chambers, vector drift chambers, and multidrift chambers and straw tubes. These detectors are widely used, in particular, as vertex detectors.

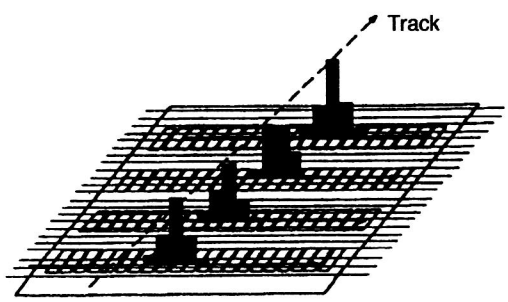

FIG. 7. Profile of the charge induced at the pads of a time-projection chamber.

TIME-PROJECTION CHAMBERS

One of the earliest TPCs is described in Refs. 10 and 11. At first glance, the TPC has a simple construction. It is usually shaped as a cylinder, which is filled with a mixture of argon and methane. The beam pipe of the accelerator passes through the center of it. A central conducting membrane at a potential of 150 kV divides the cylinder into two halves. At the chamber end caps are MWPCs with cathode readout, which are divided into six segments. In turn, each segment contains 192 proportional wires arranged at an angle relative to the radial direction of the chamber. The wire spacing is 4 mm.

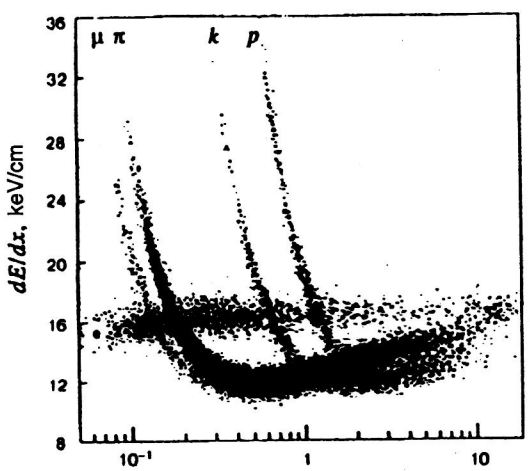

FIG. 8. Dependence of the energy loss on the particle momentum.

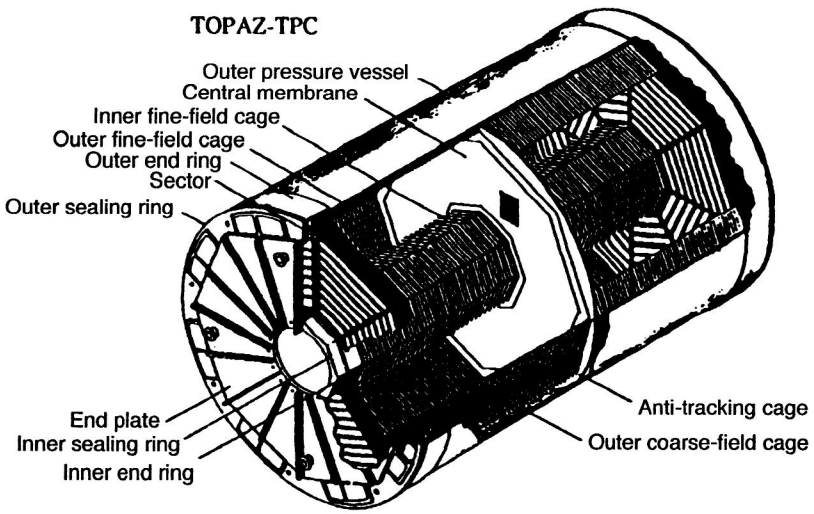

FIG. 9. General view of the TOPAZ time-projection chamber.

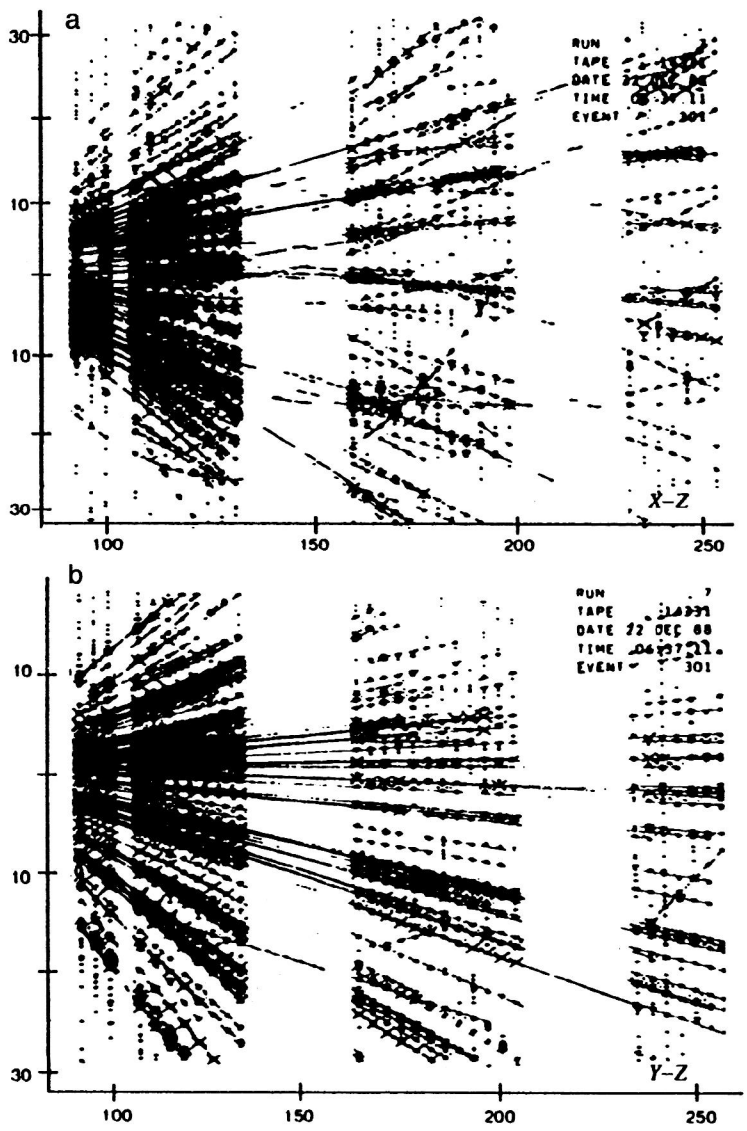

FIG. 10. An event consisting of 102 tracks: (a) projection on the $x-z$ plane; (b) projection on the $y-z$ plane; (c) projection on the $x-y$ plane; (d) view rotated by 180°.

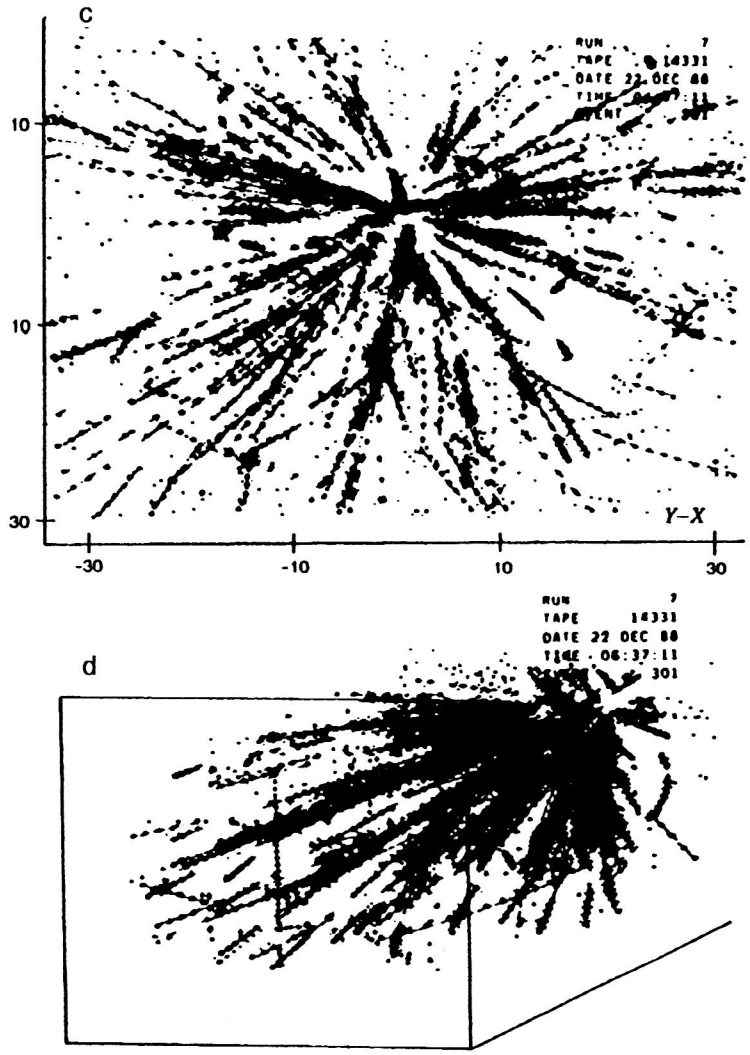

FIG. 10 (*Continued.*)

Each wire corresponds to a cathode strip divided into 12 pads of area 0.8×0.8 mm^2. The cylinder is located in a magnetic field. As a result of ionization of the gas mixture by a charged particle, groups of electrons are formed along the particle trajectory which drift in the electric field with a velocity of order 50 μm/nsec in the direction of the MWPC, where they are detected. The two coordinates r and ϕ are determined from the location of the strips and wires, and the third coordinate z is determined by the time for electrons to drift along the beam axis. Therefore, three coordinates are measured for each track. The dipole magnet performs two functions: it deflects charged particles in the plane of the MWPC so that the particle momentum can be measured and it reduces the diffusion of ionization electrons. The track detector detects these electrons as they approach the electrodes of the MWPC. The use of modern electronics allows hundreds of tracks to be recorded with high resolution (hundreds of μm). As an example, in Fig. 5 we show a complicated event recorded using the PEP-4 multiwire chamber at Berkeley.[12] The characteristics of this chamber are given in Table II. The number of recording channels in the chamber is 16 020, of which 2196 serve as proportional wires and 13 824 are assigned to the cathode strips. The design of a typical data channel consisting of an amplifier, an analog delay based on a CCD matrix, and a digitizing circuit is described in Ref. 13. Multichannel encoders based on memory modules are used for fast multistop time measurements.[14]

As will be shown below, rectilinear wire chambers are also used (see Fig. 6). Such a chamber consists of a large drift volume filled with gas, the passage of charged particles through which produces ionization. MWPCs with cathode readout are located at one or two faces. To record tracks in three dimensions, along with the two projected coordinates measured using the MWPCs (Fig. 7), the electron drift time is also determined. To record more than one track, the cathode plane consists of a set of pads.[15] A suitable electronic readout system amplifies and digitizes these signals (which have duration 50 nsec), and transfers them for further analysis. Owing to the chamber size and the electron drift time (50 μm/nsec), the maximum drift time can be hundreds of microseconds. In practice, this means that the data collected by TPCs cannot be used in a first-level trigger system.

A valuable feature of the TPC is the possibility of using information such as the particle energy loss (dE/dx) for particle identification (Fig. 8). This requires, especially in the relativistic region, a resolution of better than 3%. The key to solving this problem is the possibility of obtaining up to

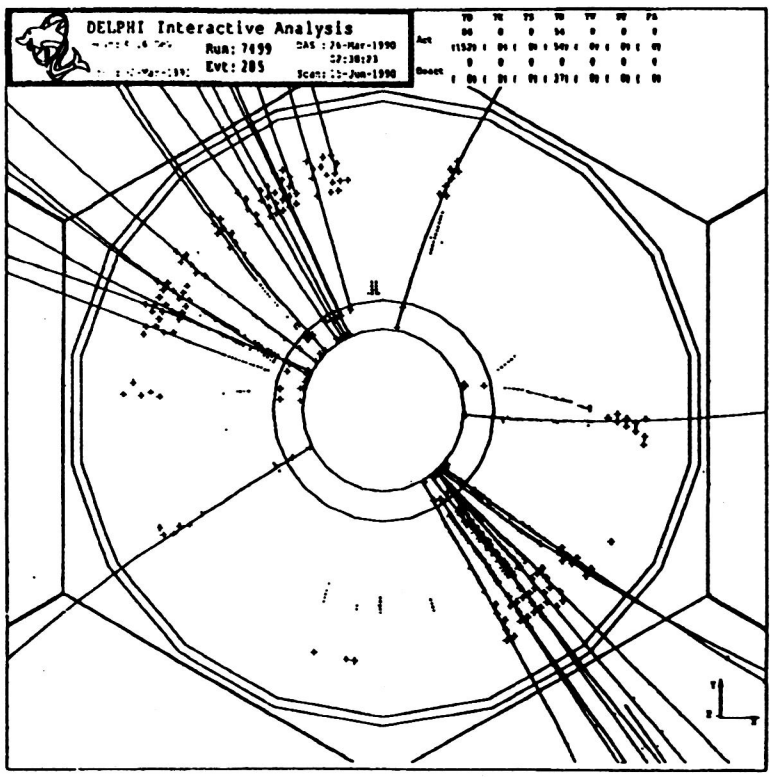

FIG. 11. Display showing the passage of a particle through the microvertex detector, the inner detector, and the closest section of the DELPHI time-projection chamber.

hundreds of independent measurements of dE/dx for each track by measuring the charge collected at the sense wires. Moreover, by using fast ADCs with a digitizing frequency of up to 100 MHz (Ref. 16), it is possible to accurately measure also the signal shape, which allows improvement of an important parameter: the two-track resolution. Below we shall discuss the features of several TPCs used in large-scale detector systems.

The TOPAZ TPC. The PEP-4 TPC became the prototype for the development of several other detectors of this class which took advantage of advances in the technology used for physics experiments. The TOPAZ TPC is described in Ref. 17. In it the cathode pads used to record azimuthal ϕ coordinates are larger than in the PEP-4 chamber and, importantly, have a zig-zag arrangement, allowing higher accuracy of coordinate determination for a smaller number of signal channels. The construction of the electrodes of this chamber is described in more detail in Ref. 18. A general view of the TOPAZ TPC is given in Fig. 9. The chamber was designed to perform e^+e^- experiments at the TRISTAN accelerator and ensures good momentum resolution ($\Delta p/p = 1\%$ of p for $p > 2$ GeV/c) and high dE/dx of order 4%. After amplification and shaping, analog signals are read out at a frequency of 10 MHz using CCD matrices, and after buffering are digitized by means of ADCs. A FASTBUS system is used to process the digital data and transfer them to a computer. In addition, an original trigger system and specialized processor for determining the coordinates of decay vertices were developed for the TPC and the jet chamber located inside (see below).

The HISS TPC. A rectilinear TPC was built at Brookhaven (BNL). It consists of three modules, and is designed to be used in a beam of heavy relativistic ions at high particle multiplicity (of order 100). In Fig. 10 we show the reconstruction of an event containing 102 tracks. Good two-track resolution is obtained owing to the large number of independent readout channels using specialized integrated circuits. In particular, a system of short (1 cm) anode wires arranged parallel to the beam and a gas mixture with low diffusion coefficient are used.[19] The use of short anode wires allows more accurate measurement of the parameter dE/dx used for particle identification at high multiplicity.

The HISS TPC represents an improved version of the rectilinear TPC. It is also designed to study multiple events occurring in relativistic ion collisions,[20] but with much higher multiplicity (multiplicity $t \sim 200$). The parameters of

TABLE III. Some characteristics of the ALEPH TPC.

Resolution in the $r-\phi$ plane	160 μm for pad intersection angle 0°		
	400 μm for pad intersection angle 10°		
Resolution of the z coordinate in the polar angle:	90°	45°	20°
for pads, mm	0.7	1.7	2.3
for wires, mm	3	2	2
Momentum resolution $\Delta p/p^2$	1.5×10^{-3}(GeV/c)$^{-1}$		
Resolution dE/dx	4.5% for 280 wires		

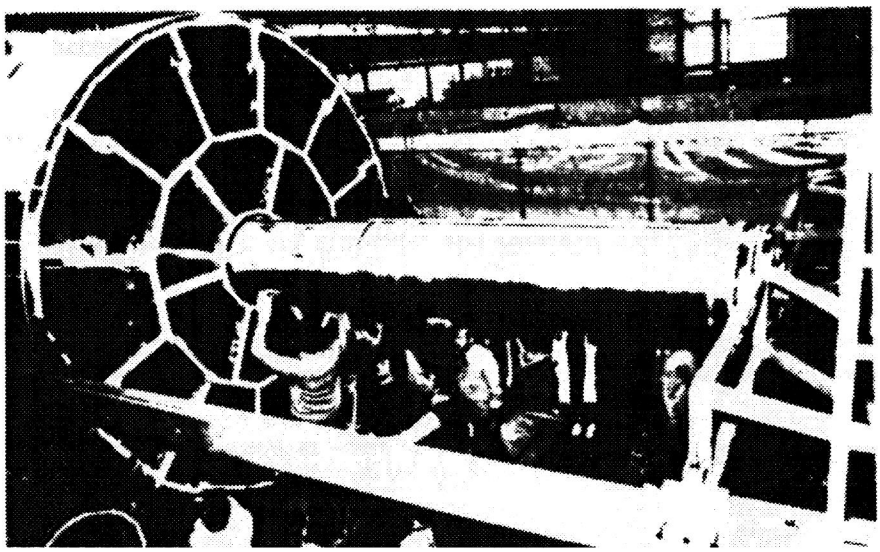

FIG. 12. General view of the ALEPH time-projection chamber in the particle beam channel.

this chamber are given in Table II. The HISS chamber, which has an active region of $150\times96\times75$ cm^3, is designed to operate at atmospheric pressure. It is located between the poles of a magnet. The electrons drift from one side of the MWPC with cathode readout, and on the other side there is a planar electrode at high potential. Between them is a rectilinear grid chamber 15 cm high, ensuring stability of the detector and uniformity of the field in the cathode plane. The chamber is held at a voltage of kV. The cathode plane contains 15 360 pads of area 1.2×0.8 cm^2, which occupy an area of 150×95 cm^2. The anode wires are held at a voltage of 1170 V and ensure a gas multiplication factor of order 3000.

A special feature of the recording electronics of the HISS TPC is that not only the amplifiers, but also such circuits as the shapers, analog memory, and multiplexers are located right on the cathode plane. The analog signals are stored in a multichannel specialized microcircuit consisting of a matrix of switched microcapacitors fabricated by CMOS technology. Data readout using CCD matrices is also possible.

The TPC operating at the JINR. A detector based on proportional chambers (PCs) with a drift gap is described in Refs. 21 and 22. It, together with the multichannel readout and recording electronics, essentially amounts to a TPC. The device consists of two modules: an input PC and a PC with a drift gap. The input PC is designed to determine the y and z coordinates of a particle as it enters the detector. The second module is used to measure such quantities as the ionization along the particle path, the particle mean free path (if the particle stopped inside the module), the electron drift time, which allows the determination of the particle trajectory in the xz plane perpendicular to the wires, and the division of the avalanche charge on the Ohmic resistance of several signal wires, which gives the y coordinate of the points on the track. This device is a good tool for the identification and spectrometry of slow particles. Filled with helium, it can serve as a proton and deuteron polarimeter.

The DELPHI TPC. The TPC of the DELPHI setup is the principal track detector and performs the functions of the central detector. The chamber has the following dimensions: radius $R=120$ cm, length $L=2\times150$ cm, and useful volume 14 m^3. The face where the MWPC is located is divided

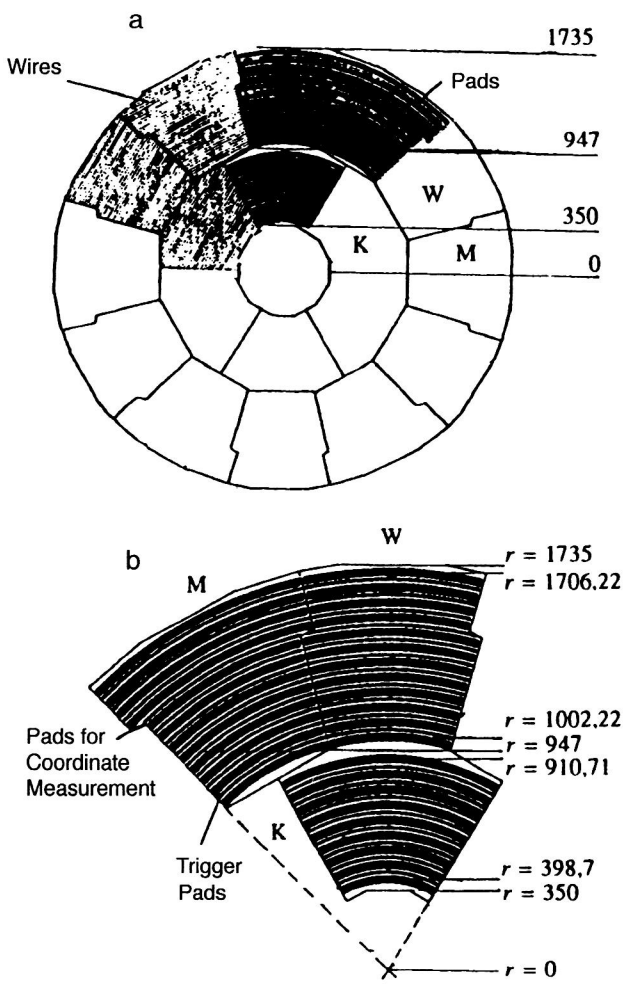

FIG. 13. (a) Geometry of the cathode plane of the ALEPH time-projection chamber. (b) A more detailed view of the M, W, and K sectors.

into six sectors, each containing 192 sense wires and 16 pads. Preamplifiers are located directly on the MWPC. After two-cascade amplification, the signals are fed to the inputs of 8-bit parallel ADCs, which digitize the signals with a frequency of 14 MHz. Six miniature lasers are also located on the chamber face to mimic tracks during detector diagnostics.

Tests of the TPC used in the DELPHI setup[23,25] gave the following parameter values: drift velocity 64 μm/nsec, resolution $\sigma(dE/dx)=(5.5\pm0.5\%)$, resolution in the $r-\phi$ plane 180–280 μm, and two-track resolution 1.5 cm. The information read out from the TPC is also used to organize a trigger signal and to reconstruct tracks by means of a specialized track processor based on the well known contiguity-mask algorithm.[24] The central detector performs the following functions: (1) measurement of the coordinates of particle tracks; (2) effective e/π separation; (3) measurement of particle momenta (in conjunction with inner and outer semiconductor vertex detectors). In FIg. 11 we show an event recorded using the DELPHI tracking system, consisting of a semiconductor vertex detector, an internal jet chamber, and the TPC.

The ALEPH TPC ("ALEPH: A detector for LEP Physics"). The TPC of the ALEPH collaboration is the largest chamber designed for experiments at LEP. In general, the apparatus was designed for solving a wide range of problems, in particular, for the detailed study of the parameters of the Standard Model of weak interactions such as the decay modes and products of the Z^0 and $W^{\pm}$ bosons, to test QCD at large Q^2, to search for the top quark, and so on.[24–26] The TPC is used directly as a track detector to measure charged-particle momenta and emission angles with high resolution and to determine the ionization density dE/dx used to separate pion and electron tracks. The z coordinate is obtained by measuring the drift time for known drift velocity equal to 5.2 cm/μsec, and the $r-\phi$ coordinate is found by interpolating the signals read out from the pads. The pad location in the radial direction gives the r coordinate. The TPC and fast ADCs are used to measure 21 points for each track. The trajectory of a charged particle inside the chamber volume is

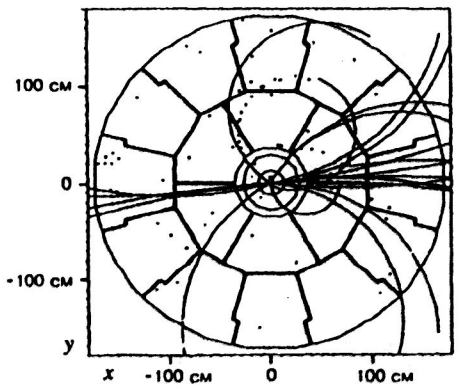

FIG. 14. An event recorded on-line using the ALEPH time-projection chamber.

a helix, and arcs or circles are obtained upon projection on the chamber faces. The spatial resolution of the ALEPH TPC has been measured[26] as 150 ± 5 μm. In Table III we give some important characteristics of this TPC (see also Table II).

The ALEPH TPC forms a part of the large central detector containing the inner tracking chamber and the TPC. The TPC is cylindrical (Fig. 12) with axially parallel magnet and electric fields. In the center of the chamber there is a membrane dividing the chamber into halves. Electrons produced by a charged particle passing through the chamber drift toward one of the chamber faces, where the sensitive electrodes of MWPCs are located. The MWPCs located at the chamber faces are divided into 18 sectors. As an example, in Fig. 13a we show the geometry of the face detector (MWPCs with cathode readout). In Fig. 13b we give a more detailed view of the M, W, and K sectors. The cathode pads are located 4 mm from the sense wires. Each sector contains a different number of pads, the total number of which is 41 004 (there are 6000 anode wires). Since the drift time is of order 45 μsec, the information read out from the TPC is used for level-2 event selection. The analog signals are digitized using parallel ADCs and stored in a buffer. Each event

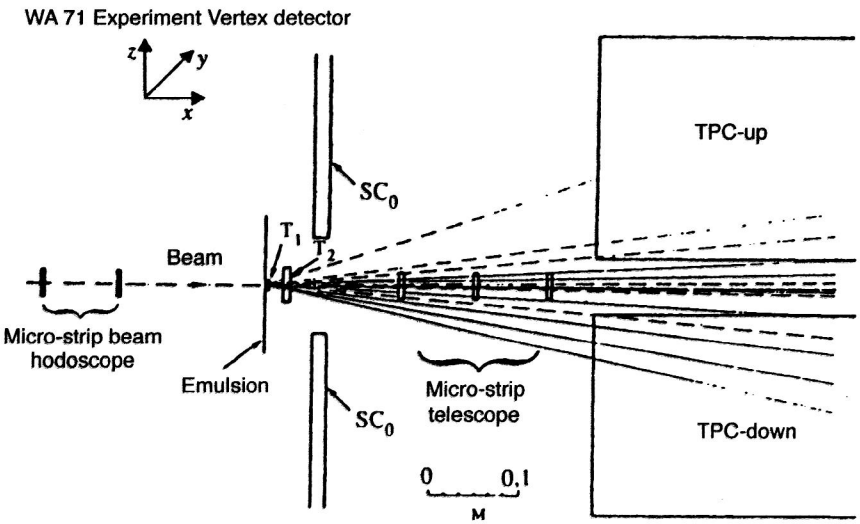

FIG. 15. Schematic depiction of the WA71 spectrometer.

TABLE IV. Parameters of the TPC used in the WA71 experiment.

Characteristic	Value
Anode wire diameter	20 μm
Cathode wire diameter	100 μm
Field wire diameter	100 μm
Spacing of anode wires	12 mm
Proportional gap	6 mm
Drift gap	160 mm
Pad area	6×8 mm^2
Number of anode wires	16
Number of pad columns	3
Number of pads per column	32
Gas mixture	70% argon+29% isobutane +1% isopropyl alcohol

corresponds to 25 Mbytes of data.[28] An important feature is that the track information obtained using this chamber is processed by a neutral network.[29] Qualitative images of particle tracks are obtained in the off-line mode; one is shown in Fig. 14.

The TPC used in the WA71 experiment. TPCs are often used in a part of a detector where the particle tracks are less dense and the tracks correspond to large emission angles. These TPCs operate in conjunction with smaller detectors of higher resolution. In the experiment described in Refs. 30 and 31, two rectilinear TPCs operate in conjunction with a microstrip silicon telescope. The chambers are located in the magnetic field of an Omega spectrometer and form a part of the vertex detector shown schematically in Fig. 15. It is designed to search for bottom particles produced in emulsion bombarded by a 350 GeV/c π^--meson beam. The microstrip telescope is used to record the particle coordinates with high accuracy at small angles $\theta\leqslant90$ mrad. The two-track resolution is 150 μm. The TPC is designed to record particle tracks in the range $65\leqslant\theta<600$ mrad. An important feature of this TPC is the thinness of the material (in units of the radiation length) used in the chamber construction. The main parameters of the TPC are given in Table IV.

The particle momenta and values of dE/dx were measured using 7-bit parallel ADCs. The accuracy of determining the decay vertex is 800 μm on the z axis and 1 mm on the x axis (the beam direction).

The TPC for the CDF experiment. The vertex TPC used in the CDF (Collider Detector at Fermilab) experiment[32] is one of the main track detectors used for collider experiments at Fermilab. The TPC consists of eight double TPCs (modules) which surround the beam pipe (Fig. 16) and are shifted relative to each other by 11.3°. Each module has a central grid at high voltage which divides the module into two drift regions, each of length 15.25 cm. For a drift velocity of 46 μm/nsec the maximum drift time is 3.5 μsec, which corresponds to the time between beam crossings of 3.5 μsec. Electrons drift from the center of the grid, pass through the cathode electrodes, and reach the MWPC wires. The sensitive area of the endcaps is divided into octants, each containing 24 sense wires and 24 cathode pads. The main parameters of the TPC are given in Table II. The basic functions performed by the vertex TPC are the following: (1) finding the z coordinate of the decay vertex; (2) reconstructing the topologies of all events within the polar angle $3.5°\leqslant\gamma\leqslant176.5°$; (3) reconstructing the tracks in high-multiplicity events; (4) detecting charged particles near the interaction vertex, where the amount of matter is small; (5) recording tracks in the angular range $10°\leqslant\theta\leqslant30°$. In this range the data obtained from the TPC and the central detector are used both to record tracks, and to measure momenta; (6) the information obtained from the MWPC wires is used in the $r-z$ plane for the preceding calorimeter, and so on.

USE OF CHAMBERS OF THE JET TYPE

TPCs have a number of important drawbacks: a relatively low response rate, which is determined by the drift time, and difficulty in identifying events in regions of high track density. The more complicated detectors of the jet type are free of these problems. Jet chambers (microvertex detectors) are usually located right at the beam pipe. They are often referred to as inner drift chambers, because they are located inside TPCs. The review by Saxon[33] is devoted to the history of the development of the jet chamber and improved three-dimensional gas detectors—vertex detectors. The pro-

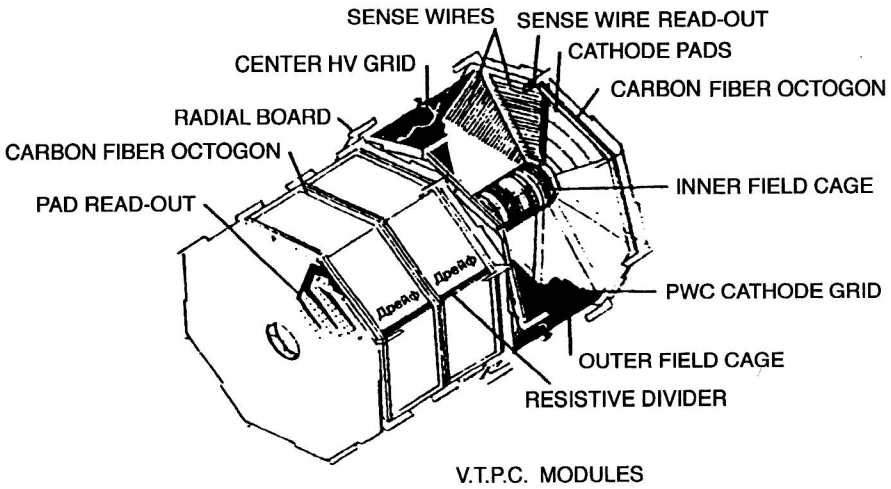

FIG. 16. General view of the CDF time-projection chamber.

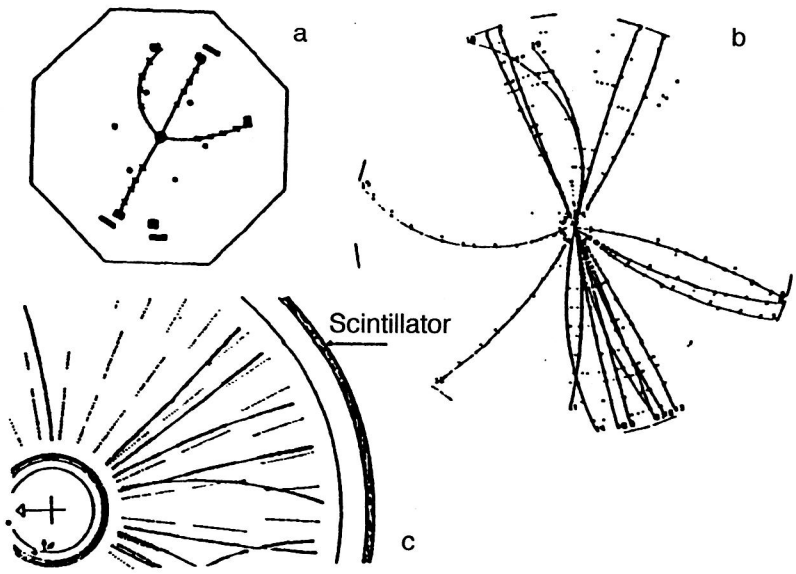

FIG. 17. (a) The decay $\psi' \to \psi\pi^+\pi^-$ recorded by four concentric spark chambers (the MARK I detector). (b) An event $e^+e^- \to$ hadrons, recorded by the TASSO detector containing 2340 drift cells. (c) A typical event recorded using the JADE jet chamber.

totype is the MARK I detector, which consists of four cylindrical spark chambers. This detector has been used to record the decay $\psi' \to \psi\pi^+\pi^-$ (Fig. 17a). The ever-increasing particle energy, momentum, and event multiplicity has stimulated the improvement of three-coordinate gas detectors. There are two basic trends in this development. In the MARK II setup, the detector consists of four concentric layers, each filled with a set of independent drift cells. Accurate measurement of three coordinates in z, r, and ϕ space is possible (Fig. 17b). This technique has also been widely used in other spectrometers. For example, the detector in the TASSO setup[34] contains 15 layers (2340 cells) with a drift gap of 16 mm. The improved JADE detector, referred to as a pictorial chamber,[35] has length 2.4 m, outer diameter 1.6 m, and inner diameter 0.4 m. The detector volume is divided into 24 independent segments forming a bicycle-wheel geometry. In turn, each segment viewed in the radial direction consists of four drift cells with 16 anode wires in each cell. The left–right ambiguity is resolved by shifting the sense wires by a few hundred microns relative to each other. The high density of sensitive points in the chamber volume ensures the reconstruction of events with even higher multiplicity (Fig. 17c).

The concept of pictorial chamber has become widespread and has stimulated the development of efficient data-acquisition electronics and specialized processors. The response rate of this class of three-coordinate gas detectors is an order of magnitude higher than that of TPCs. We shall illustrate this by some particular examples. We shall also give a brief description of the construction of the best known microvertex detectors of the jet type.

The TOPAZ microvertex detector (Ref. 36). This setup has 4π geometry and is designed to detect charged and neutral particles at the TRISTAN accelerator in Japan. It consists of TPCs, time-of-flight counters, and an inner jet chamber. The microvertex chamber used in the TOPAZ setup performs the following functions: (1) the organization of fast trigger signals; (2) precision measurement of the track positions in the $r-\phi$ and $r-z$ planes. Special construction techniques are used to achieve these goals. In particular, the chamber contains 10 layers of drift cells. In the azimuthal direction, the four inner layers have 64 and the six outer layers have 128 drift cells. Eight layers of zigzag-type delay lines are used as cylindrical cathodes to accurately measure the z coordinate. To efficiently select tracks using specialized processors, the search is performed independently in the $r-\phi$ and $r-z$ planes. In Fig. 18 we show the block diagram of the electronics. Preamplifiers fabricated using hybrid technology with a gain of 200 for the anode lines and 7500 for the delay lines are located right at the detector. Signals are sent via twisted pairs of leads 25 m long to the inputs of discriminators, which split the logic signals with the TTL-level signal for the track-finder modules and the ECL differential signal for the TDCs. The signals obtained from the jet chamber are primarily used to organize the pretrigger for the spectrometer. Since the beam-crossing interval at the accelerator where this detector is used is 2.5 μsec, the decision-making device must have a maximum dead time of 2 μsec. This response rate is achieved both owing to the chamber geometry and construction, and by use of tabulated solutions.

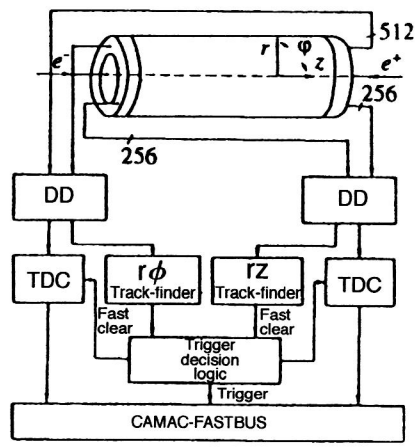

FIG. 18. Block diagram of the electronics for the TOPAZ jet chamber. DD are discriminator–dividers and TDC are time-to-amplitude converters.

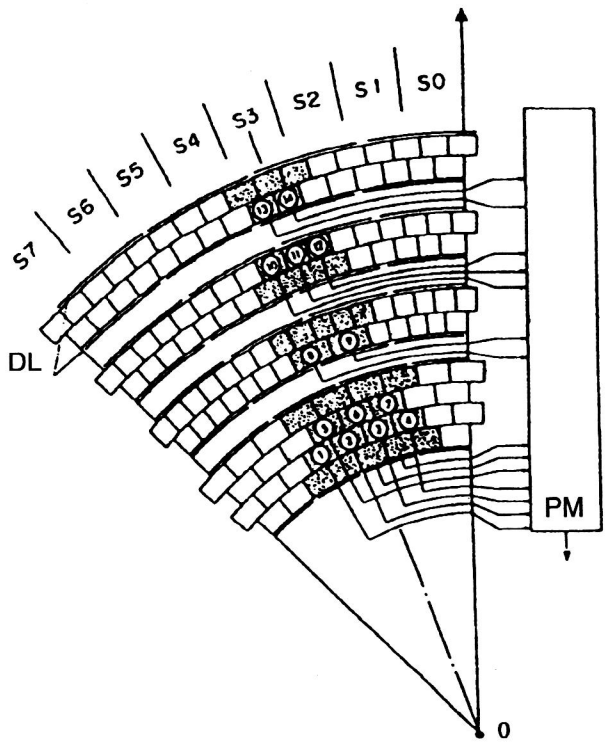

FIG. 19. Structure of the cells used to seek tracks in the $r-\phi$ plane. Si are the detector sectors, DL is the delay line, and PM is programmable memory (look-up table).

In Fig. 19 we show the structure of the anode cells used to seek tracks in the $r-\phi$ plane. The coincidence signals from two adjacent layers are used to obtain the pulses T1-T15. The cells located in the corresponding layers are grouped together in azimuthal angle, forming 64 sectors. A sector, shown in Fig. 19, consists of 4-3-2-3-2 cells. First, the images of the most probable tracks are written in memory (a look-up table), and then, if they coincide with the recorded tracks, after 150 nsec a coincidence signal is generated. The tabulated trajectory images can be changed if necessary. The method of seeking tracks in the $r-z$ plane is explained in Figs. 20a and 20b. The delay lines are located on eight radial layers and separated into 32 segments in the azimuthal direction. Each segment has its own track finder. The logic scheme of the track finder is based on TDC modules, majority logic, and shift registers. Let us briefly discuss the operation of the track finder. The first signal sent from one end of the delay line triggers a pulse-pack generator. By measuring the signal arrival time, the side, right or left of the interaction point, on which the track is located is found. The signals from the other end of the delay line are read into a shift register; the shift frequency is variable, depending on the location of the delay line. After all the signals are read using majority logic, the number of units recorded in the radial direction is analyzed and, if it is equal to the preset value, a signal is generated. The time for seeking a track in the $r-z$ plane is made up of the following: the maximum electron drift time (250 nsec), the time for the signal to propagate in a half-length of the delay line (260 nsec), the delay in the cables (130 nsec), the delay in the discriminator-divider modules (50 nsec), the decision time of the track processor (750 nsec), and the processing time of the majority logic (60 nsec). Coincidence of the signals generated in the two track finders is used to send the information obtained from the TDC modules to the second-level trigger decision logic, where the search for the event vertices is carried out. The information received from the TPC and the system of time-of-flight counters is also used here in the following way.[37] The proportional chamber located at the TPC face is divided into eight sectors with 176 sense wires in each sector. Each sector has its own track finder. The 88, out of the 176, wires located closest to the beam are used for track reconstruction. To improve the noise stability, they are connected using OR elements to form 11 groups, at the outputs of which signals W1–W11 are generated upon passage of a track (Fig. 21). These signals are sent to the logic chain (Fig. 22). Since the signals are sent at different times, to obtain coincidence they must be delayed appropriately. It is easy to see that a signal appears at the output of RW1 when signals appear simultaneously at the inputs of RW1 and RW2. In other words, the scheme shown in Fig. 22 reconstructs particle tracks. For this it is sufficient to note the two time points RW1 and RW6. Here it is assumed that the tracks have small curvature. After the tracks are found in a different processor, the coordinates of the decay vertices are located (Fig. 23). The vertex processor is based on shift registers in which time marks corresponding to the found track are stored, and the data obtained in this manner including correction factors are compared to masks whose images are stored in a memory module of volume 256 Kbytes. The accuracy of recording the coordinates of a decay vertex is 10 cm, and the calculation time is 30 μsec.

The jet chamber in the OPAL setup (Refs. 38 and 39). This microvertex chamber is used in conjunction with a track processor in the OPAL spectrometer to find the primary

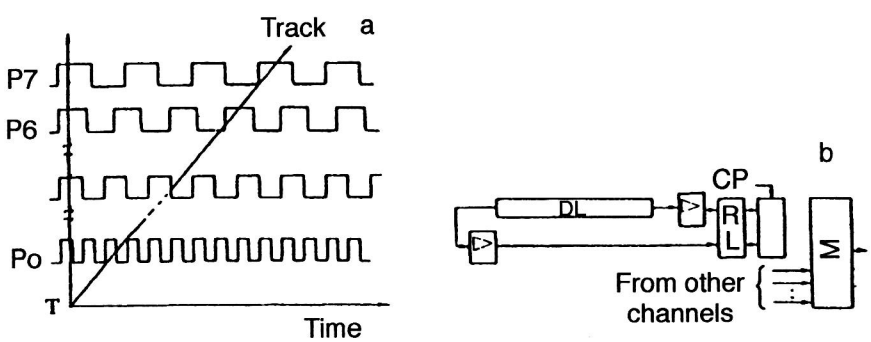

FIG. 20. Explanation of the method of seeking tracks in the $r-z$ plane: (a) clock pulses used for shifting data from delay lines to shift registers; (b) the track finder: DL—delay line, R—right, L—left, CP—clock pulses, RG—shift register, M—majority logic.

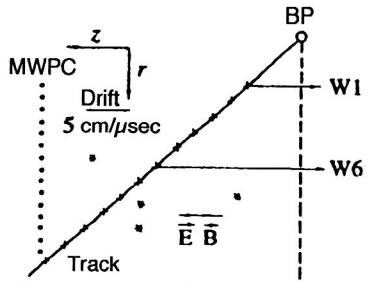

FIG. 21. Signals used from the MWPC wires of the time-projection chamber. BP is the beam pipe, and W1–W6 are data channels.

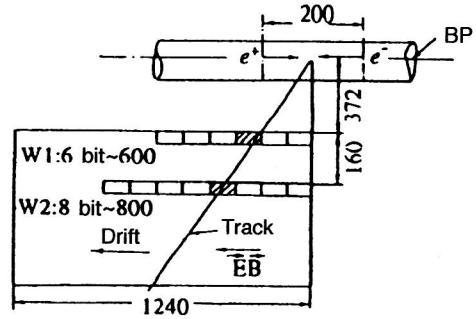

FIG. 23. Scheme for determining the primary interaction coordinates. BP is the beam pipe.

decay vertex and for particle identification. The trigger is organized using information on such physical processes as (1) e^+e^-, (2) $q\bar{q}$, (3) $\gamma\gamma$, (4) $\tau^+\tau^-$, (5) $\mu^+\mu^-$, (6) $e^+e^-q^+q^-$, and (7) various exotic events. Events (1)–(3) are detected by a calorimeter and therefore are used directly to organize the trigger. Since events (4)–(7) release a small amount of energy, their detection and reconstruction requires a specialized processor with a decision time of at least 22 μsec (the bunch-crossing period).

The vertex detector consists of a small, high-precision drift chamber right next to the beam pipe and a second jet chamber which surrounds the small chamber (Fig. 24). The small chamber has diameter 47 cm and length 100 cm, and is located in a magnetic field of 0.4 T. Each chamber has 36 cells in the $r-\phi$ direction; the cell structure is shown in Fig. 25. We see that a drift cell of the inner chamber covers 10° in the direction of the ϕ coordinate and contains 12 anode sense wires with radius between 103 and 162 mm. The outer rings of stereo cells oriented at an angle of 5° relative to the z axis each have six such wires with radius between 188 and 213 mm. Altogether there are 648 sense wires. The microvertex chamber operates at a pressure of 4 bar and contains a gaseous mixture of argon, methane, and isobutane in the ratio 89:8:3. The drift velocity is 45 μm/nsec, the gas gain is 10^5, and the maximum drift gap is 20 mm. This ensures an accuracy of 50 μm of finding particle coordinates in the $r-\varphi$ plane by means of time-amplitude transformers, while the accuracy on the z axis is 3 cm. The z coordinate is determined by calculating the difference in the arrival times of signals from the wire ends. The large jet chamber is 4 m long and is divided into 24 sectors in the azimuthal direction (ϕ). Each sector contains 159 axial sense wires. Let us describe how the jet chamber is used in the design of an effective track processor.[41] It was found that the simplest tracks leaving the interaction vertex lie in the $r-z$ plane. The operating principle of the processor can be explained using Fig. 26. If a track leaves the interaction vertex, the ratio z/r is a constant for all the layers of the chamber. Tracks are found from the peak in the histogram, which is calculated using a fast processor. A detailed description of the trigger system of the entire setup and the readout and recording electronics can be found in Refs. 39–41. An improved track processor is described in Ref. 41. Along with histogram construction, it uses a systolic processor and transformation of variables based on the Hoff transform. The calibration procedure used to measure the particle energy loss is described in Ref. 42. A resolution of 3–4% is obtained, allowing the identification of particles accompanying Z^0 decay with momentum up to 20 GeV/c. In Fig. 27 we give the energy-loss curves in multihadron and dimuon events as a function of the particle momentum.

The microvertex detector for the UA1 experiment. A precision jet chamber has been built for the well known UA1 experiment. The pressure of the working gas is 3 atm and the resolution per wire is 50 μm. The small distance (1.58 mm) between the sense and potential wires ensures the sampling of up to 16 coordinates over a radial distance of 5 cm (Ref. 43). The main parameters of the jet chamber are given in Table VI. The chamber is divided into 16 cells in the azimuthal direction. Each cell contains 16 sense wires, between which are located wires producing an electric field. The sense wires are shifted relative to the field-producing wires

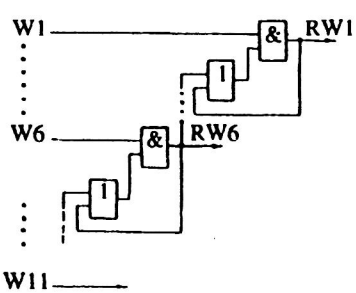

FIG. 22. Logic chain used for "extending" a track.

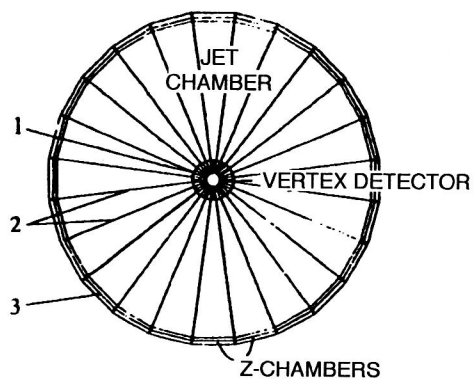

FIG. 24. Schematic depiction of the OPAL jet chamber in the $r-\phi$ plane. (1) Small jet chamber (microvertex detector); (2) second jet chamber; (3) external drift chambers.

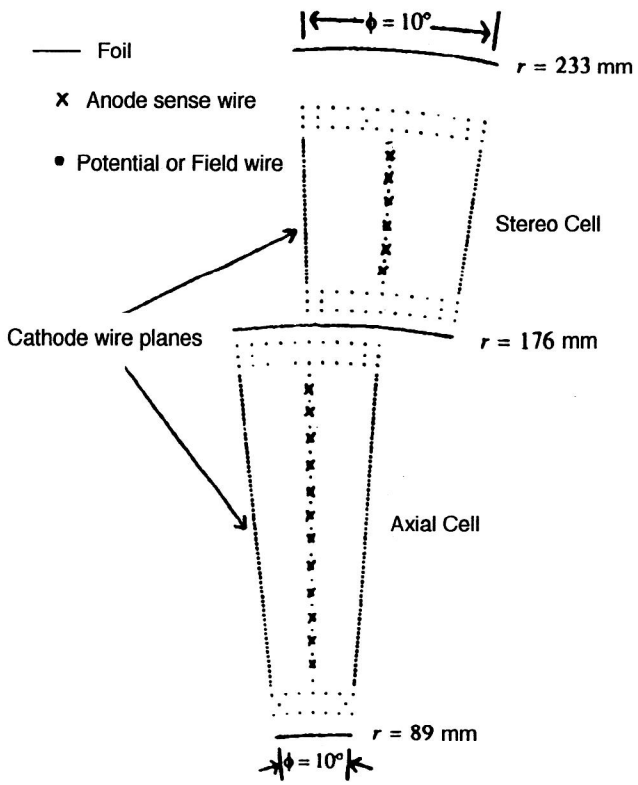

FIG. 25. Geometry of one axial and one stereo cell of the OPAL jet chamber.

by 100 μm, which allows resolution of the left–right ambiguity. The maximum drift gap is 16 mm, which ensures good track resolution. Stable operation of the detector in a collider beam for three weeks was demonstrated in 1985.

The jet chamber for the UA2 experiment. This detector is a cylindrical drift chamber located close to the beam pipe, where an inner semiconductor vertex detector is placed. It is designed for the UA2 experiment[44] and allows very accurate measurement of particle tracks near the beam pipe, where short-lived particles decay. The chamber has been operating successfully at CERN since 1987. In Fig. 28 we show the geometry of one of the 16 sectors of this chamber. In Table V we give the main parameters of this detector.

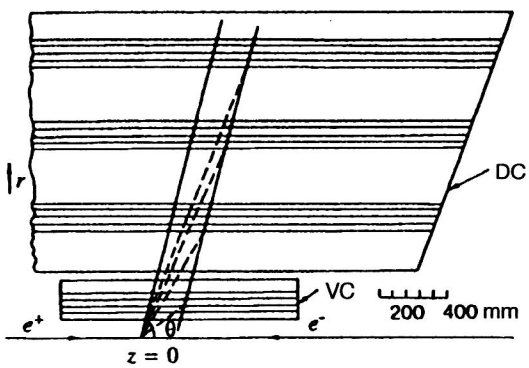

FIG. 26. Method of reconstructing the coordinate of a decay vertex in the OPAL vertex detector in the $r-z$ plane. DC is the drift chamber, VC is the vertex chamber, and Z is the interaction point.

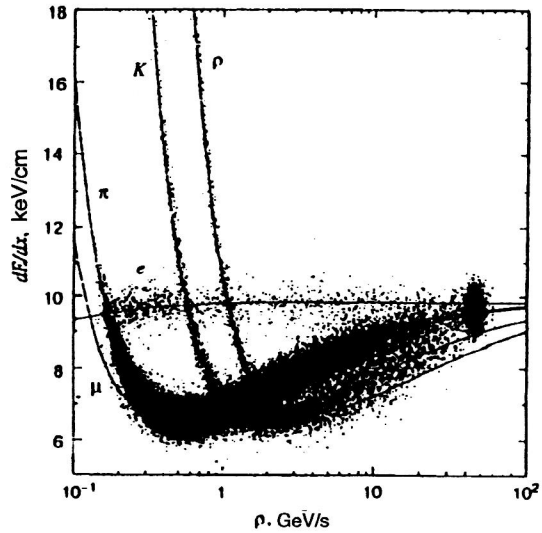

FIG. 27. Dependence of dE/dx on the particle momentum.

In order to resolve the left–right ambiguity, adjacent sense wires, the distance between which is 6.44 mm, are shifted relative to each other by ± 200 μm. In Fig. 29 we show a two-track event reconstructed using the time-of-flight electronics on the basis of measurement of the electron drift time. The signals were digitized using 6-bit parallel ADCs. We see that even when the momenta overlap, the radial coordinate of a particle is determined quite accurately. The distance between the centers of mass is 4 mm, and the maximum drift time is 500 nsec.

The MARK II microvertex detector (Refs. 45 and 46). This detector is designed to record and study Z^0 decays by identifying heavy colored quarks and to measure the lifetime of heavy quarks and leptons at the Stanford Linear Accelerator (SLAC). The main problem in designing the detector was to obtain a high spatial resolution of order 30 μm and good two-track resolution of at least 1000 μm. These problems were solved by specially controlling the pressure and temperature inside the chamber, and also by careful construction

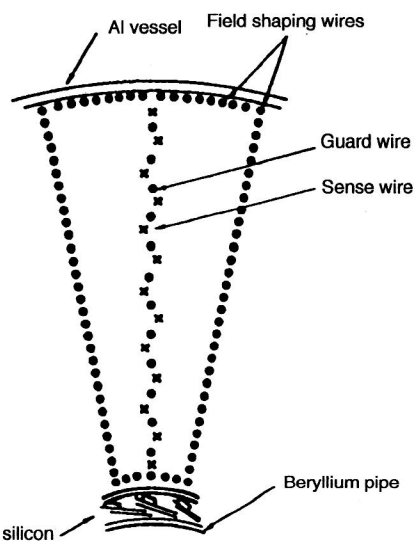

FIG. 28. Geometry of a sector of the UA2 jet chamber.

TABLE V. Parameters of the UA2 jet chamber.

Parameter	Value
Sensitive length	1000 mm
Inner radius	34 mm
Outer radius	128.5 mm
Inner sensitive radius	40 mm
Outer sensitive radius	123.8 mm
Number of sectors	16
Number of wires per sector	13
Wire spacing	6.44 mm
Wire displacement	0.2 mm
Gas mixture	60% argon+40% ethane
Pressure	1 atm
Drift velocity	51.8 ∓ 0.3 μm/nsec
Electric field	−1.05 kV/cm

of the chamber and drift cells. The active region of the detector has length 55 cm in the azimuthal direction and from 5 to 17 cm in the radial direction. The chamber volume is divided into 10 jet cells arranged in the radial direction. This feature of the cell geometry simplifies the resolution of the left–right ambiguity, ensures measurement of the drift velocity in the calibration process, and provides better quality of track recording.

Each cell contains an anode plane consisting of sense wires of diameter 20 μm, with potential wires of diameter 225 μm located between them. At the cell boundaries there are grid planes of wires of diameter 150 μm which decrease the crosstalk and increase the stability of the electric field of the sense wires, which are separated from each other by 2.9 mm. The grid (guard) plane is located 1.8 mm from the anode plane. The chamber operates at a pressure of 3 atm for a gas mixture of 92% CO_2+8% C_2H_6. The cathode planes consisting of wires of diameter 225 μm are located between the guard planes. The high voltage ensures an electric field of 2.3 kV. Signals are read out and digitized using parallel ADCs operating at a frequency of 100 MHz.

In Table VI we give the main parameters of jet-type chambers and vector drift chambers.

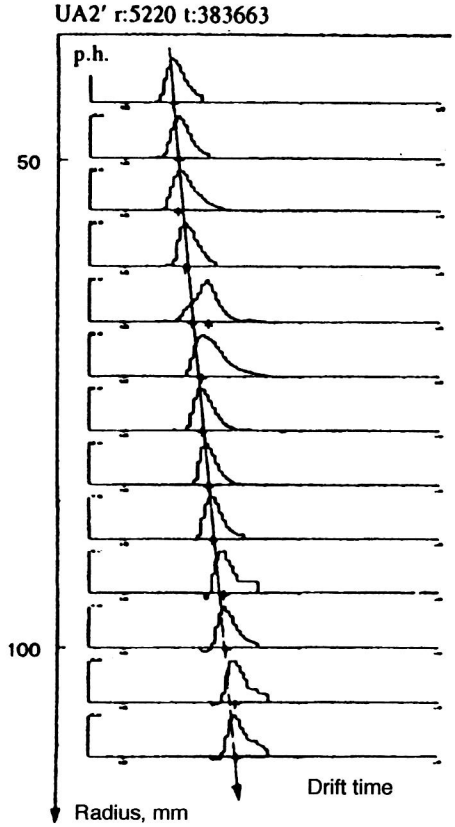

FIG. 29. Example of the use of a jet chamber for track reconstruction. The distance between the centers of gravity of the momentum distribution is 4 mm.

The large cylindrical chamber for the VENUS detector. The VENUS detector is a general-purpose detector for experiments at the TRISTAN accelerator, whose energy is 70 GeV (Refs. 47 and 48). The main track detector in the setup is a cylindrical drift chamber. In order to record events with high multiplicity (>20) and narrow jets with a spatial resolution of 150–200 μm, special attention was paid to the structure of the drift cells. The prototype was the PEP-4 jet chamber. The chamber has inner radius 25 cm, outer radius

TABLE VI. Parameters of chambers of the jet type.

Experiment	MARK II [45.46]	MARK J [55–56]	SLD [53]	CDF [53]	ZEUS [50]	H1 [52]	ALEPH [27]	OPAL [38–41]	TOPAZ [36,37]	UA1 [43]
Radius, mm:										
inner	192	100	200	277	162	200	160	89	106	25
outer	1440	242	961	1320	785	769	260	233	293	89
active	250	–	238	309	190	215	–	–	–	–
Active length, mm	2300	576	1800	3214	2050	2400	2000	1000	1500	800
Number of layers	72	–	80	84	72	64	8	2	10	–
Number of superlayers	12×16	–	10×8	12+6 +6	9×8	2×32	–	–	–	–
Number of sense wires	5832	168	5120	6156	4608	2560	960	648	–	256
Stero angle	3.8°	–	1.7°	3°	5°	7°	–	–	–	–
Maximum drift gap, mm	33	27.5	26	35	25	51	20	–	16	–
Drift velocity, μm/nsec	52	7	9	50	50	35	49	52.7	–	51
Maximum drift time, nsec	600	–	3000	700	500	1500	140	5800	–	–
Magnetic field, T								0.435		
Sampling frequency, MHz								100		

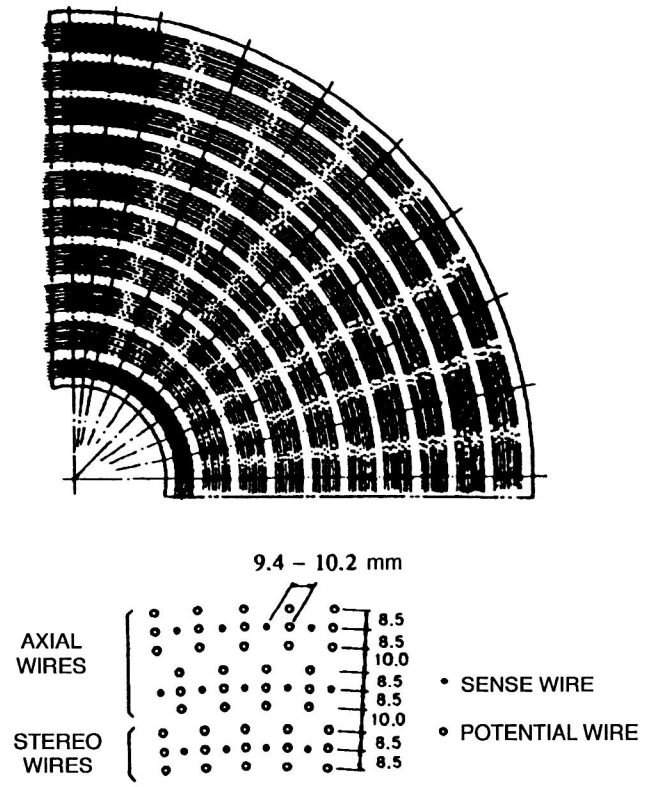

FIG. 30. One quarter of the chamber and geometry of a drift cell of the TRISTAN jet chamber.

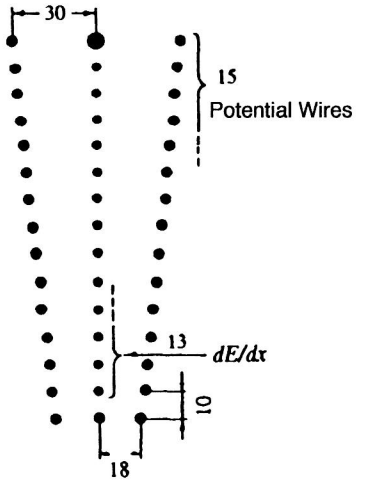

FIG. 31. Geometry of a drift cell of an inner layer of the MARK III vector drift chamber.

126 cm, and length 300 cm. The total number of sense wires is 7104, and there are 21 312 potential wires. In Fig. 30 we schematically show a quarter of the chamber and the cell geometry.[47] There are 20 axial layers of drift cells for measurements in the $r-\phi$ projection (the plane perpendicular to the beam axis). Moreover, every two layers, which are shifted relative to each other by half a cell, form a double layer. Since in such a pair of layers each particle triggers two times, it is possible to measure the particle coordinates in the $r-\phi$ plane and along the track. This allows clearer recognition of tracks with large curvature and resolution of the left–right ambiguity, and it increases the chamber efficiency as a whole. The method of reconstructing tracks in the off-line mode is described in Ref. 49.

Other types of jet chamber. A prototype of the microvertex detector for the ZEUS setup has been developed and tested at the HERA accelerator.[50] Collisions between 1 TeV protons and 30 GeV electrons are expected to give a large flux of heavy colored particles generated by the electroweak interaction. Charm and bottom particles have a mean free path of the order of several microns in the $r-\phi$ plane transverse to the beam. The microvertex chamber has been designed taking this into account. The outer radius of the chamber is 159 mm and the inner radius is 99 mm. A drift cell has three radial planes: the central plane contains 13 field wires with 12 sense electrodes between them, and the two side planes each contain 25 drift wires. The angle of 1.5° between the planes gives a drift gap ranging from 2.6 to 3.6 mm. An efficiency of 96% and a spatial resolution of 35 μm in the central region of the chamber are obtained.

The ARGUS drift chamber is designed for experiments in the e^+e^- storage ring of the DORIS-II accelerator.[51] A solenoidal magnet ensures a magnetic field of 0.8 T. A drift chamber and time-of-flight and shower counters are located inside the solenoid. The experiment is designed also to study bottom mesons, including exclusive reactions with high multiplicity. The problem was how to ensure a high momentum resolution in the range from 50 MeV/c to 5 GeV/c.

PROSPECTS FOR FUTURE DEVELOPMENT

Vector vertex detectors. Further improvement of three-coordinate gas detectors has focused on raising the quality of reconstructing tracks with large curvature, and also determining the track direction. These chambers are called vector drift chambers.[33] They have a multilayered structure. As examples, let us consider the CDF and MARK III vector chambers.

The CDF vector chamber is a large drift chamber designed to perform experiments in high magnetic fields with a high density of curved tracks at the hadron collider at Fermilab.[53] The detector has a complicated geometry. It contains 84 layers arranged into 9 superlayers. The five superlayers whose wires are parallel to the beam axis each contain 12 sense-wire layers. These five axial layers are interleaved with four superlayers of stereo wires, in which the angle between the sense wires and the beam axis alternates between $\pm 3°$. Each stereo superlayer contains six sense-wire layers. Both the axial and the stereo superlayers are divided into drift cells, so that the maximum drift distance is less than 40 mm, which corresponds to a drift time of 800 nsec. In Table VI we give the main parameters of the CDF vertex detector.

The vector drift chamber in the MARK III spectrometer[54,55] has eight layers. The first layer forms a small drift chamber with four layers. The second layer is essentially a jet chamber consisting of 32 drift cells (Fig. 30). It has a dense grid of sense cells, allowing the reconstruction of curved tracks and highly accurate measurement of dE/dx. A characteristic feature of superlayers 3–8 is the presence of

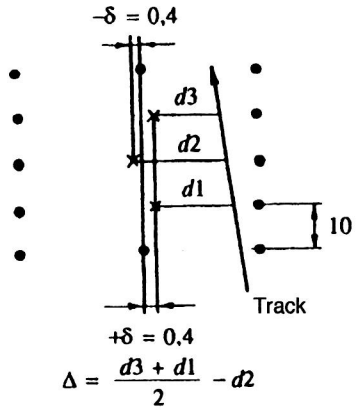

FIG. 32. Geometry of a drift cell of one of the outer layers of the MARK III vector drift chamber.

three sense wires shifted by 300 μm in each drift cell (Fig. 31). The method of seeking tracks in vector drift chambers is described in Ref. 54. Both software and hardware methods are used for fast and efficient track searching, and they ensure the complete reconstruction of events containing tracks of large curvature in 37 msec. The manner of resolving the left–right ambiguity is illustrated in Figs. 31 and 32. For the triplet of wires shifted by $\pm\delta$, the value of Δ determining the distance a charged particle travels from the sense wire is given by[54]

$$\Delta = v_d[(t_1+t_3)/2-t_2],$$

where t_1, t_2, and t_3 are the measured times for particles passing through the cell. We see from Fig. 33 that Δ has two peaks, and its sign tells which side of the cell the particle passed.

Microvertex detectors with time expansion (Refs. 57–59). Drift chambers with time expansion (time-expansion chambers) are also used for highly accurate measurement of the impact parameter (up to 100 μm). Their features are the following:[55] (1) the presence of a region of low field strength (the drift velocity is 5 μm/nsec compared to the 50 μm/nsec in ordinary jet chambers) separated from a region of high field strength; (2) the use of parallel ADCs with a digitizing frequency of 100 MHz for more accurate determination of the drift time by determining the center of mass; and (3) the use of a gas mixture with as small a diffusion coefficient and small Lorentz angle as possible. An example of a detector of

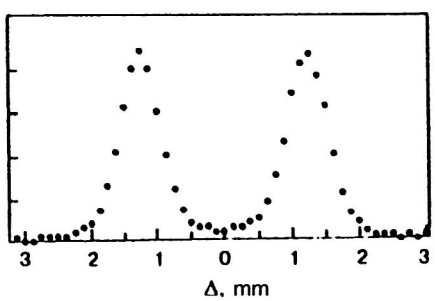

FIG. 33. Distribution of Δ as a function of where the particle passes relative to the drift cell. The two peaks correspond to tracks passing to the left and right of the cell.

TABLE VII. Basic parameters of the MARK J time-projection chamber.

Parameter	Value
Inner diameter, mm	100
Outer diameter, mm	242
Sensitive length, mm	576
Number of segments	12
Number of sense wires per segment	14
Total number of sense wires	168
Distance between anodes, mm	2.4
Distance between potential wires, mm	2.54
Distance between grid electrodes, mm	0.6
Drift velocity, μm/nsec	7.0
Gas mixture	80%CO_2+20%CH_4
Spatial accuracy, μm	35

this type is the jet chamber MARK J, designed for experiments at DESY. In Table VII we give the main parameters of this detector.

A time-expansion chamber has also been used in the L3 experiment,[59] where a resolution per wire of 51 μm and a two-track resolution of 650 μm were obtained. The operating principle of the chamber is explained in Fig. 34, where we show the cell geometry. The electron drift region is divided into a region with small uniform field and a region with large electric field (the multiplication region), where the sensitive plane is located. These regions are separated by a plane held at zero potential. Between the anode wires there are focusing wires, which increase the two-track resolution. The main parameters of the chamber are the following: outer and inner diameters equal to 937 and 170 mm, respectively, length equal to 1260 mm, and maximum drift time of less than 10

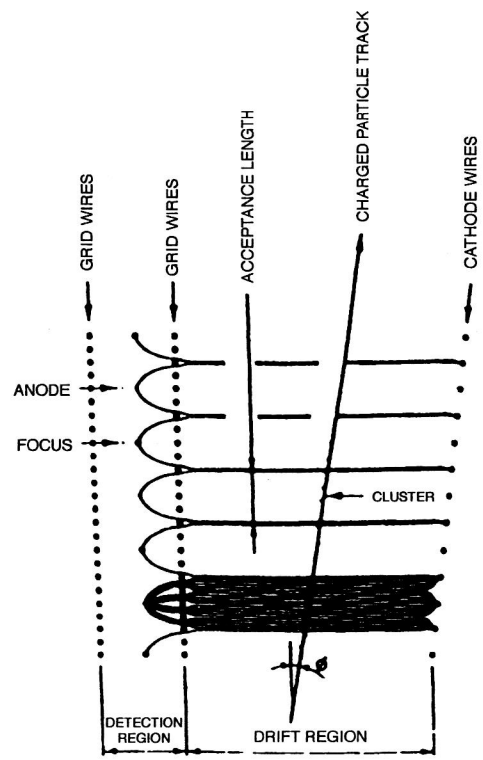

FIG. 34. Sketch of a cell of a time-expansion chamber.

TABLE VIII. Parameters of detectors with straw tubes (Ref. 62).

Experiment	HRS	MAC	MARK II	MARK III	CLEO	TPC	AMY
Tube diameter, mm			8.0	8.0	5.9–7	8	5.3–5.9
Length, cm	41–46	43	75	84	51	40–60	56
Wire diameter, μm	20	30	20	50	15	30	15
Wire thickness, μm	85	100	75	75	32	100	38
Number of tubes	352	324	552	640	192	984	144
Resolution, μm	100	45	90	49	90	50	85
Pressure atm	1	4	1	3	1	4	1.5
Gas	At/Et	$ArCo_2$	CH_4Ar/Et	Ar/Et	Ar/Et	$ArCo_2CH_4$	Ar/Et
Voltage, kV	1.65	3.9	1.9	3.9	1.6	4	1.75

μsec. The chamber volume is divided into two concentric cylinders: an inner cylinder containing 12 sectors and an outer cylinder containing 24 sectors. The maximum drift gap is 35.4 mm for the inner chamber and 53.2 mm for the outer one.

Detectors with precision cells. Another direction in the evolution of fast, precision three-dimensional gas detectors is the development of drift cells with high resolution. There are two original designs in this area. The authors of Ref. 60 describe two chambers, one based on a set of square drift cells of dimensions 21×21 mm^2 with a drift gap of 10.5 mm, and and the other using hexagonal drift cells with a drift gap of 25 mm. A spatial resolution of 25–30 μm was obtained. It has been shown that this trend in the development of precision three-coordinate gas detectors, with cells which form a cylindrical drift field, used in conjunction with a gas mixture with low diffusion, is more promising than that of time-expansion chambers owing to the simpler construction of the detector.

MULTIDRIFT AND STRAW TUBES

An original line of development is the use of multidrift tubes.[61] The problem is to design a precision three-dimensional gas detector operating in high beam luminosity (10^{33}) with a short memory of order 30–50 nsec. The drift cells are hexagonal and are combined into modules. A module consists of a set of drift tubes of radius 1.45 mm. Seventy such cells are located in a tube of diameter 30 mm and length 80 cm. Each anode wire corresponds to six cathode wires. A detector containing 8000 resistive anode wires has been built from such modules. The accuracy of positioning the wires is better than 30 μm. The problems arising in the use of multidrift tubes as vertex detectors at high charge loads are discussed in Ref. 62. In particular, it is essential to develop a new approach to designing the recording electronics. Since the dead time is of order 50 nsec and sampling of up to 50 times per track can be done, such a detector can be used as a trigger system.

Straw tubes. Another promising development in the design of fast, precision vertex detectors is detectors incorporating thin Mylar tubes of diameter 3–5 cm and thickness 25–300 μm. At the center of a tube of length 45–100 mm is an anode wire, and the aluminumized wall of the tube serves as the ground bus. These detectors possess the following attractive features: (1) relatively low cost; (2) in contrast to classical drift chambers, straw tubes are isolated from each other, and so damage to one tube does not affect the operation of the others; (3) reduced effect of crosstalk; (4) a small drift time of 30–100 nsec; (5) high accuracy (several μm) of recording coordinates. An important drawback of these detectors is the presence of an additional material, Mylar, which tends to decrease the momentum resolution of the detector. Studies are being carried out in order to reduce the effect of multiple scattering.[63] The parameters of several detectors based on straw tubes are given in Ref. 64 (see Table VIII).

As an example, let us consider in more detail the construction of the MARK III microvertex chamber.[65] In Fig. 34 we show the cross section of part of the chamber. It consists of 12 concentric layers of tubes located between radii of 5.4 cm and 13.0 cm from the interaction point. There are 640 tubes altogether, and the tube diameter is 8 mm.

The method of reconstructing tracks and their intercepts for the straw-tube drift chamber in the E735 experiment is described in Ref. 66. The principle of the track reconstruction is shown in Fig. 35. Here we see two layers of tubes with radii r_1 and r_2. Tracks 1–4 satisfy the following system of equations:

$$\sin(t)(X_2-X_1)-\cos(t)(Z_2-Z_1)+(r_2-r_1)=0$$

$$\sin(t)(X_2-X_1)-\cos(t)(Z_2-Z_1)-(r_2-r_1)=0$$

$$\sin(t)(X_2-X_1)-\cos(t)(Z_2-Z_1)-(r_2+r_1)=0$$

$$\sin(t)(X_2-X_2)-\cos(t)(Z_2-Z_2)+(r_2+r_1)=0.$$

After calculating t, the slope $\tan(t)$ and intercept are calculated for each line. After the equation of a line is found, it is projected to the next chamber, and compared with the measured coordinate. If the difference is less than a given value, the hit is tagged as belonging to the line. The χ^2 criterion is used.

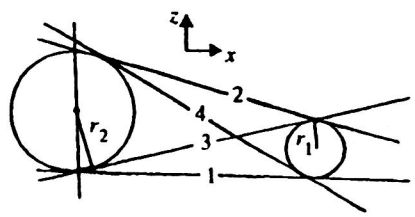

FIG. 35. Explanation of the algorithm for reconstructing straight tracks recorded using straw tubes.

CONCLUSION

The technique of three-coordinate gas vertex detectors in conjunction with the readout electronics and computational methods of selecting and reconstructing the topologies of complicated events has become highly refined. Detectors of this class are distinguished by their radiation stability, their good two-track resolution, and their relatively fast response. Moreover, the possibility of recording events with large particle emission angle allows the successful use of three-dimensional gas vertex detectors in combination with other types of detector in the high-luminosity experiments performed at modern and future colliders. Gas microstrip microvertex detectors based on semiconductor technology are also very promising and have been discussed in our earlier review.[67]

[1] C. J. H. Damarell, Preprint RAL-86-077, Rutherford Appleton Laboratory, Chilton (1986).
[2] H. Crote, Rep. Prog. Phys. **50**, 475 (1987).
[3] S. Petrero and G. Romano, Nucl. Instrum. Methods **170**, 61 (1980).
[4] G. I. Barber, A. T. Belk, Beuselink *et al.*, Preprint ALEPH-IC-88-12, Blackett Laboratory, London (1988).
[5] S. Gadomski and M. Turala, Nucl. Instrum. Methods Phys. Res. A **344**, 125 (1994).
[6] P. F. Manfredi and F. Ragusa, Nucl. Instrum. Methods Phys. Res. A **252**, 208 (1986).
[7] Yu. V. Zanevskiĭ, *Multiwire Proportional Chambers* [in Russian] (Atomizdat, Moscow, 1975).
[8] G. Charpak, Phys. Today **31**, No. 10, 23 (1978).
[9] A. H. Walenta, J. Heintze, and B. Schurlein, Nucl. Instrum. Methods **92**, 373 (1971).
[10] J. Heintze, Nucl. Instrum. Methods **156**, 227 (1978).
[11] D. R. Nygren and J. N. Marx, Phys. Today **31**, No. 10, 46 (1978).
[12] F. Sauli, Preprint CERN-EP/89-74, CERN, Geneva (1989).
[13] H. Aihara, M. Alston-Garnjost, D. H. Badtke *et al.*, IEEE Trans. Nucl. Sci. **NS-30**, 162 (1983).
[14] K. Eggert, Cl. Engster, L. Van Koningsveld *et al.*, Nucl. Instrum. Methods **176**, 223 (1980).
[15] F. Sauli, Preprint CERN-PPE/94-195, CERN, Geneva (1994); P. Bock, J. Heintze, T. Kunst *et al.*, Nucl. Instrum. Methods Phys. Res. A **242**, 237 (1986).
[16] M. Atiua, M. Ito, J. Haggerty *et al.*, Nucl. Instrum. Methods Phys. Res. A **279**, 180 (1989).
[17] T. Kamae, H. Aihara, R. Enomoto *et al.*, Nucl. Instrum. Methods Phys. Res. A **252**, 423 (1986).
[18] T. Miki, R. Iton, and T. Kamae, Preprint Ut-HE-84/2, Tokyo (1984).
[19] A. Etkin, S. E. Eseman, K. J. Foley *et al.*, Nucl. Instrum. Methods Phys. Res. A **283**, 557 (1989).
[20] G. Rai, A. Arthur, F. Bieser *et al.*, Preprint LBL-2841, Lawrence Berkeley Laboratory, Berkeley (1990).
[21] Yu. Zlomanchuk, A. Navrot, V. A. Nikitin *et al.*, Prib. Tekh. Éksp. No. 5, 53 (1982) [Instrum. Tekh. Eksp.].
[22] A. A. Budilov, Yu. V. Zanevskiĭ, Yu. Zlomanchuk *et al.*, Prib. Tekh. Éksp. No. 2, 48 (1985) [Instrum. Tekh. Eksp.].
[23] C. Brand, S. Cairanti, P. Charpentier *et al.*, Nucl. Instrum. Methods Phys. Res. A **283**, 567 (1989).
[24] G. Darbo and B. W. Heck, IEEE Trans. Nucl. Sci. **NS-34**, 227 (1987).
[25] P. Aarnio, H. Abie, P. Areu *et al.*, Nucl. Instrum. Methods Phys. Res. A **303**, 233 (1991).
[26] S. R. Amendolia, T. Barczewski, L. A. T. Bauerdick *et al.*, Nucl. Instrum. Methods Phys. Res. A **283**, 573 (1989).
[27] D. Decamp, B. Deschieaux, J.-P. Lees *et al.*, Nucl. Instrum. Methods Phys. Res. A **294**, 121 (1991).
[28] S. R. Amendolia, F. Fidecaro, A. Lusiani *et al.*, Nucl. Instrum. Methods Phys. Res. A **289**, 569 (1990).
[29] G. Stimpl-Abele, Comput. Phys. Commun. **64**, 46 (1991).
[30] S. Benso, G. Darbo, L. Rossi *et al.*, Nucl. Instrum. Methods Phys. Res. A **217**, 194 (1983).
[31] M. Dameri, G. Darbo, E. Lamana *et al.*, Nucl. Instrum. Methods Phys. Res. A **235**, 279 (1985).
[32] F. Snider, M. Binkley, J. Huth *et al.*, Nucl. Instrum. Methods Phys. Res. A **268**, 75 (1988).
[33] D. H. Saxon, Preprint RAL-87-022, Rutherford Appleton Laboratory, Chilton (1987).
[34] H. Boerner, H. M. Fischer, H. Hartman *et al.*, Nucl. Instrum. Methods **176**, 151 (1980).
[35] H. Drumm, R. Eichler, B. Granz *et al.*, Nucl. Instrum. Methods **176**, 333 (1980).
[36] A. Imanishi, T. Ishii, S. Kato *et al.*, Nucl. Instrum. Methods Phys. Res. A **269**, 513 (1988).
[37] R. Enomoto, K. Tsukauda, N. Ujiie *et al.*, Nucl. Instrum. Methods Phys. Res. A **269**, 507 (1988).
[38] A. A. Carter, J. R. Carter, R. D. Heuer *et al.*, Nucl. Instrum. Methods Phys. Res. A **250**, 503 (1986).
[39] A. A. Carter, J. R. Carter, J. C. Hill *et al.*, Nucl. Instrum. Methods Phys. Res. A **286**, 107 (1990).
[40] F. Klefenz, W. Conen, R. Zoz *et al.*, in *Proceedings of the Intern. Conf. on Computing in High Energy Physics*, CERN 92-07, CERN, Geneva, p. 251.
[41] M. Arignon, A. H. Ball, K. W. Bell *et al.*, Nucl. Instrum. Methods Phys. Res. A **313**, 103 (1992).
[42] M. Hauschild, R.-D. Heuer, C. Kleinwort *et al.*, Preprint CERN-PPE/91-130, CERN, Geneva (1991).
[43] Th. Müller, Nucl. Instrum. Methods Phys. Res. A **252**, 387 (1986).
[44] F. Bosi, G. Carboni, V. Cavasinni *et al.*, Nucl. Instrum. Methods Phys. Res. A **283**, 532 (1989).
[45] G. Hanson, Nucl. Instrum. Methods Phys. Res. A **252**, 343 (1986).
[46] J. P. Alexander, R. Baggs, D. Fujino *et al.*, Nucl. Instrum. Methods Phys. Res. A **283**, 519 (1989).
[47] R. Arai, H. Boerner, N. Ishihara *et al.*, Nucl. Instrum. Methods Phys. Res. A **217**, 181 (1983).
[48] Y. Yamada, K. Hayshi, N. Ishihara *et al.*, Preprint 92-166, KEK, Ibaraki-ken, Japan (1992).
[49] T. Oyama, T. Horose, K. Amako *et al.*, Nucl. Instrum. Methods Phys. Res. A **305**, 71 (1991).
[50] C. Alvisi, G. Anzino, F. Azzarello *et al.*, Nucl. Instrum. Methods Phys. Res. A **305**, 30 (1991).
[51] M. Danilov, H. Hasemann, P. Kim *et al.*, Nucl. Instrum. Methods **217**, 153 (1983).
[52] G. A. Beck, J. B. Dainton, E. Gabathuler *et al.*, Nucl. Instrum. Methods Phys. Res. A **283**, 471 (1989).
[53] F. Bedeshi, J. P. Berge, J. Bofill *et al.*, Nucl. Instrum. Methods Phys. Res. A **268**, 50 (1988).
[54] J. Roehrig, K. Einsweiler, D. Hutchinson *et al.*, Nucl. Instrum. Methods **226**, 319 (1984).
[55] D. Bernstein, J. Bernstein, K. Bunnell *et al.*, Nucl. Instrum. Methods **226**, 301 (1984).
[56] J. J. Becker, J. S. Brown, and D. Coffman, Nucl. Instrum. Methods Phys. Res. A **235**, 502 (1985).
[57] H. Anderhub, H. Anders, S. Ansari *et al.*, Nucl. Instrum. Methods Phys. Res. A **252**, 357 (1986).
[58] H. Anderhub, H. Anders, S. Ansari *et al.*, Nucl. Instrum. Methods Phys. Res. A **263**, 1 (1988).
[59] H. Anderhub, W. Bauer, F. Beauvais *et al.*, Nucl. Instr. and Meth., V. **332**, 34 (1993).
[60] V. Commichau, K. H. Dederichs, M. Deutschmann *et al.*, Nucl. Instrum. Methods Phys. Res. A **239**, 487 (1985).
[61] R. Boucler, G. Charpak, and G. A. Erskine, Nucl. Instrum. Methods Phys. Res. A **283**, 509 (1989).
[62] F. Sauli, Preprint 88-02, CERN, Geneva (1988).
[63] V. Aulchenko, A. G. Chilingarov, G. M. Kolachev *et al.*, Nucl. Instrum. Methods Phys. Res. A **283**, 528 (1989).
[64] W. H. Toki, Preprint SLAC-PUB-5232, SLAC, Stanford (1990).
[65] J. Adler, T. Bolton, K. Bunnell *et al.*, Nucl. Instrum. Methods Phys. Res. A **276**, 42 (1989).
[66] S. H. Oh, D. K. Wesson, J. Cooke *et al.*, Nucl. Instrum. Methods Phys. Res. A **303**, 277 (1991).
[67] N. M. Nikityuk, Fiz. Élem. Chastits i Atom. Yadra **28**, No. 1, 191 (1997) [Physics of Particles and Nuclei **28**, 77 (1997)].

Translated by Patricia A. Millard